



# Management and optimization of Grid-tied Renewable Energy for EV Charging Station

**Sohankumar Prajapati<sup>1\*</sup>, Sanjay R Vyas<sup>2</sup>**

<sup>1</sup>Research Scholar, Electrical Engineering Department, KadiSarvaVishwavidyalaya, Gandhinagar, Gujarat, India

<sup>2</sup>Professor, Electrical Engineering Department, L.D.R.P Institute of Technology and Research, Gandhinagar, Gujarat, India

\*Correspondence: email address sgp.gec@gmail.com

Received 17 October, 2023; Revised 5 December, 2023; Accepted 5 December, 2023

Available online: 6 December, 2023 at [www.atlas-tjes.org](http://www.atlas-tjes.org), doi: 10.22545/2023/00236

**Abstract:** *Integrating electric vehicle (EV) charging stations with renewable energy systems has garnered significant attention in recent literature. Studies frequently need optimization models for station locations incorporating renewable energy. The paper proposes employing Human-Driven Instruction-Based Optimization (HDIBO) for control strategies to address these gaps. HDIBO leverages human insights alongside algorithmic precision, enabling dynamic responses to changing conditions. This approach optimizes control strategies iteratively, bridging the gap between theoretical algorithms and real-world complexities, ensuring efficient energy management, grid integration, and EV charging optimization. The objectives of the proposed work include enhancing charging station profitability, increasing renewable energy utilization, mitigating peak grid stress and optimizing battery energy storage utilization. To validate the effectiveness of the HDIBO approach, it is compared with Genetic Algorithm (GA), Particle Swarm Optimization (PSO), and Grey Wolf Optimization (GWO) methods. HDIBO achieve improved parameter settings with lower mean and standard deviation values for efficient and stable control for the proposed system.*

**Keywords:** EV Charging management, Integration of RES, Human-Driven Instruction-Based Optimization, Economic Viability

## 1 Introduction

In the realm of EV charging stations and renewable energy systems, recent literature reveals a recurring emphasis on environmental impact assessments, particularly concerning the integration of green energy systems for charging infrastructure. However, a notable trend has surfaced, indicating that these studies often exhibit a tendency to overlook broader economic and technical

dimensions. While a wealth of research offers overviews of EV charging station technologies and design aspects, a recurring gap emerges in terms of in-depth analyses encompassing specific design considerations and the associated economic implications. Another discernible trend is the development of models aimed at optimizing station locations by incorporating renewable energy sources and storage mechanisms. Despite these efforts, there remains a consistent underrepresentation of operational and economic facets beyond the scope of location optimization. Additionally, the feasibility of hybrid solar-wind systems for EV charging stations has attracted significant attention. However, the research in this domain frequently falls short in addressing pivotal aspects such as grid stability and the intricate technical challenges entailed in the integration of diverse energy sources. A prevailing pattern emerges where investigations into hybrid renewable energy systems often narrow their focus to specific contexts, such as supermarkets with EV charging platforms. This specialization, while informative, tends to sideline the broader concerns surrounding grid integration and system-level interactions. Furthermore, studies unveiling innovative design and power management strategies for solar-powered EV charging stations underscore the need for a more comprehensive consideration of real-world operational and economic challenges faced during implementation. In essence, the recent literature unveils an evolving landscape that leans heavily on environmental assessments and design explorations yet often lacks the holistic integration of economic viability and technical feasibility that is integral to the practical advancement of EV charging station infrastructure powered by renewable sources. In (Filote et al., 2020), the environmental impact of green energy systems for EV charging, though it may overlook broader economic and technical aspects. Similarly, (Narasipuram & Mopidevi, 2021) provides an overview of EV charging station technologies but lacks in-depth analyses of specific design elements and economic implications. In (C. Li et al., 2022), a model for optimal station location incorporating renewable energy and storage is developed, but operational and economic aspects may not receive sufficient attention. A hybrid solar-wind system for EV charging, yet it may not thoroughly address grid stability and technical integration challenges evaluated in (Singh et al., 2021). While (Allouhi & Rehman, 2023) investigates hybrid renewable energy systems for supermarket charging, it might not fully consider broader grid integration concerns. Meanwhile, (Biya & Sindhu, 2019) presents a design and power management approach but may not comprehensively tackle real-world operational and economic challenges. In (Dai et al., 2019), a complex multi-agent optimization algorithm optimizes PV, battery, and EV charging designs, demanding significant computational expertise. Paper (Sayed et al., 2019) focuses on the resilient operation of a renewable-powered EV station, but broader grid integration aspects may be under-addressed. (Wu et al., 2022) Introduces the hierarchical operation of EV charging in smart grids but lacks detailed technical information and practical cases. The review of grid-connected EV station planning may not provide new empirical findings as presented in (Ma, 2019). (Yu et al., 2022) Deeply examines EV integration but may lack original empirical research. (Zandrazavi et al., 2022) Optimizes energy management in unbalanced microgrids but could overlook real-time operational challenges. (Quddus et al., 2019) Models EV charging expansion with renewable and V2G but might not fully address practical implementation. The DC bus voltage in a PV-based station, focusing on a specific context in (A. Hassoune et al., 2019). (Albert et al., 2022) Proposes an advanced EV station but does not extensively explore its limitations. An intelligent energy management scheme, but may not address all station

management aspects. In (Amir et al., 2023). A grid integration using Salp Swarm Optimization, but challenges could be further explored, as investigated in (Mohamed et al., 2020). (de Oliveira-Assis et al., 2021) Develops a microgrid system but may lack practical challenges. From (Abdelilah Hassoune et al., 2020), (Garcia-Trivino et al., 2023), (Glenn & Alavandar, 2023), (Thangam & Kalifullah, 2023), propose energy management and control strategies but do not provide comprehensive details. (Sharma & Chinnappa Naidu, 2023) Reviews optimization with retired EV batteries but may lack practical implementation insights. An neural network control for harmonics but might not fully discuss drawbacks in (Penchalaiah et al., 2023). (Saleh et al., 2021) Optimizes hybrid renewable systems with PID control but could provide more in-depth analysis. (Cabrera-Tobar et al., 2022) propose control rules to assess charging station efficacy at each time step by predictive control. In (Karmaker et al., 2023), fuzzy logic base rules develop for EV charging economic and technical performance enhancement. However no effective optimization technique implemented for better performance. In (Leonori et al., 2021), Fuzzy rule based energy management explored to fulfill power deficiency create due to unpredictable load demand of EVs and power production from renewable sources. (Khan et al., 2019), offered an improved control technique for renewable sources and grid-connected fast EV Charging AC/DC converters by operating it at unity power factor to reduce line current harmonics. (Zheng et al., 2022) propose an optimization technique PSO, GA, and BBO for to find the optimal combination of power production and energy storage modules to meet load on highway located EV Charger. In (Ray et al., 2022), the hybrid Crow Search Algorithm with PSO developed for gain more profit, reduce installation and operating cost of charging station. The green house gas emission mitigation not considered in proposed work. (Y. Li et al., 2020) presents backtracking search optimization for efficient energy scheduling in microgrid to reduce cost.

### 1.1 Research Gap

The research landscape on EV charging stations and renewable energy systems has seen significant exploration, yet certain gaps remain that warrant further investigation. While several studies have examined the environmental impact of various green energy systems for EV charging stations, there is a notable lack of research that comprehensively considers broader economic and technical aspects. Additionally, while overviews of key technologies and design aspects have been provided, the depth of analysis often falls short in addressing specific design considerations and economic implications. Moreover, though models have been developed for optimal station location by integrating renewable energy and storage, a research gap exists in fully addressing the operational and economic aspects of charging stations beyond location optimization. Similarly, studies on hybrid solar-wind systems for EV charging stations have focused largely on feasibility, overlooking crucial considerations related to grid stability and the technical challenges posed by diverse energy source integration. The scope of investigation for hybrid renewable energy systems has been limited to specific contexts, such as supermarkets and EV charging platforms, often neglecting broader grid or system integration aspects. Furthermore, research on solar-powered EV charging station design and management has centered on theoretical aspects, leaving real-world operational and economic challenges inadequately addressed. While optimization algorithms like multi-agent particle swarm optimization have been utilized; their complexities and resource demands raise concerns regarding their practical applicability. Similarly, the emphasis on resilient operation and control strategies for DC microgrid-based charging stations overlooks the need for comprehensive grid integration strategies that span both DC and AC microgrid contexts. The

overview of hierarchical operation of EV charging stations in smart grid integration highlights a research gap in technical details and practical case studies, and the same holds true for several other studies focusing on overviews and reviews rather than empirical research. Finally, comprehensive discussions about controller implications, drawbacks of proposed techniques, and real-world implementation challenges are frequently missing from the literature, leaving potential gaps in practical application unaddressed. In summary, these gaps collectively suggest a need for more holistic research endeavors that bridge theoretical models with real-world implementation challenges, encompass economic, technical, and operational considerations, and offer in-depth insights into specific design, control, and optimization strategies for EV charging stations within the broader context of renewable energy integration.

## 1.2 Employing Human Driven Instruction Based Optimization (HDIBO) For Control

Human-driven instruction-based optimized proportional-integral (PI) controllers present a promising avenue for enhancing the performance and efficiency of grid-connected electric vehicle (EV) charging stations. These controllers leverage the unique ability of human operators to intuitively understand and adapt to complex systems, infusing a level of expertise that algorithms alone may struggle to achieve. By incorporating human-driven instructions, the PI controller gains the advantage of tapping into real-time human insights, enabling it to respond dynamically to changing conditions, unforeseen scenarios, and operational nuances that arise within the charging station environment. This synergy between human intuition and algorithmic precision leads to improved control strategies that can cater to intricate interplays between renewable energy sources, grid interactions, and EV charging requirements. Furthermore, the optimized nature of the PI controller capitalizes on iterative learning and tuning processes guided by human expertise. As human operators provide feedback and insights, the controller refines its parameters, adapting its response to align with the desired objectives. This dynamic optimization empowers the grid-connected EV charging station to continuously fine-tune its energy management, load balancing, and grid interaction, thereby optimizing charging processes for both efficiency and reliability. By combining human-driven instructions with advanced optimization techniques, these controllers bridge the gap between theoretical algorithms and the operational complexity of the real world. They offer a strong and adaptable solution that maximizes the use of renewable energy, minimizes the impact on the grid, and makes sure that EV charging fits seamlessly into the larger energy ecosystem.

## 1.3 Objectives of the Proposed Work

The following are the objectives of the proposed work:

- To enhance charging station profitability through strategic measures.
- To increase renewable energy sources' contribution to load coverage.
- To mitigate peak grid stress through effective load management strategies.
- Optimizing energy storage battery unit utilization for efficiency gains

The proposed HDIBO is compared with various optimization methods, namely GA (Genetic Algorithm), PSO (Particle Swarm Optimization) & GWO (Grey Wolf Optimization), to justify the effectiveness of the work.

## 2 Methodology

As shown in Figure 1, the Grid connected Renewable energy system based Electric Vehicle charging station is made up of various components, including PV array, wind energy turbine & generator, dc-dc converter, bidirectional converter, energy storage battery, electric vehicle battery, a DC link capacitor, Voltage source inverter, Inductive filters, and other components (Glenn & Alavandar, 2023). The PV array transforms received sunlight into direct current while under MPPT control by using the peculiarities of PV cell output. Wind turbine generator convert wind energy in to electrical energy. The VSC converts the direct current (DC) electricity to alternating current (AC), which is then filtered and enhanced before being delivered into the power grid (Thangam & Kalifullah, 2023).

### 2.1 PV Array Computational Model and its Control

PV modules, in reality, link many individual PV cells to provide electrical energy. The following information describes the connection between the PV array's output current and voltage:

$$I = I_L - I_{sc} \left[ \exp - \left( \frac{q(U+IR_s)}{AKT} \right) - 1 \right] - \frac{U+IR_s}{R_p} \quad (1)$$

Where  $I_L$  stands for photo current generated and  $I_{sc}$  is for reverse saturation current. The Boltzmann constant is  $K$ , the electron charge is  $q$ , the outside temperature is  $T$ , and the diode ratio is  $A$ .  $R_p$  and  $R_s$  are the corresponding parallel and series resistances, respectively.

When subjected to direct sunlight, solar power cells transform only a tiny portion of the radiation that enters into electrical power, while the remaining heats up the module through heat transfer. Temperature and irradiance have diametrically opposed impacts on output power, and the link between solar cell heat and power output is stated as follows:

$$C_{\text{module}} \frac{dT_m}{dt} = q_{sw} - q_{lw} - q_{conv} - P_{out} \quad (2)$$

Where  $C_{\text{module}}$  is the capacity of heat in the module,  $T_m$  is the temperature of the module, and  $q_{sw}$  and  $q_{lw}$  are the shorter and longer wave rays of the light that enter the module, respectively.  $P_{out}$  denotes the output power, whereas  $q_{conv}$  denotes the heat exchange.

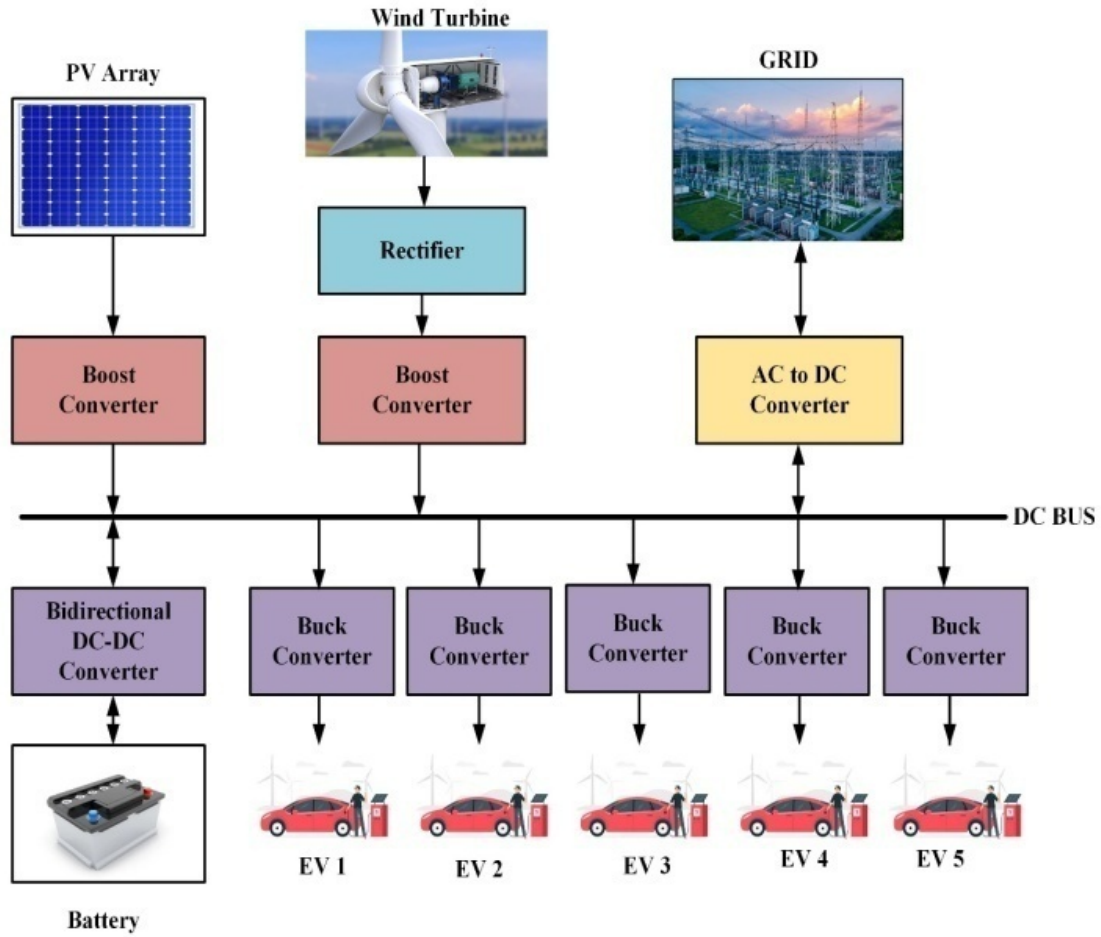


**Figure 1:**Model of Proposed system

**Table 1:** Proposed System Parameters

Sr.No	Description	Value	Units
1	PV Array		
	Rated Power	100	kW
	Voltage of single panel	36.19	V
	Current of single panel	8.43	A
	Power of single panel	305.08	W
	No series Panel	11	-
	No of Parallel String	30	-
	Boost Converter inductor	10.5	mH
	Boost converter capacitor	524	μF
	Switching Frequency	10	kHz
2	Wind Energy System		
	Rated Power	50	kW
	Maximum output Power	54	kW

	Generator Efficiency	90	%
	Boost Converter inductor	1.3	mH
	Boost converter capacitor	41	$\mu$ F
	Switching Frequency	10	kHz
3	Energy Storage Battery		
	Capacity	40	kWhr
	Nominal Voltage	300	V
	Bidirectional Converter inductor	10.5	mH
	Bidirectional converter capacitor	524	$\mu$ F
	Switching Frequency	10	kHz
4	Electric Vehicle Battery		
	Capacity	5-40	kWhr
	Nominal Voltage	300	V
	Bidirectional Converter inductor	10.5	mH
	Bidirectional converter capacitor	524	$\mu$ F
5	DC link Voltage	350	V
	Grid		
6	Voltage	400	V
	Frequency	50	Hz

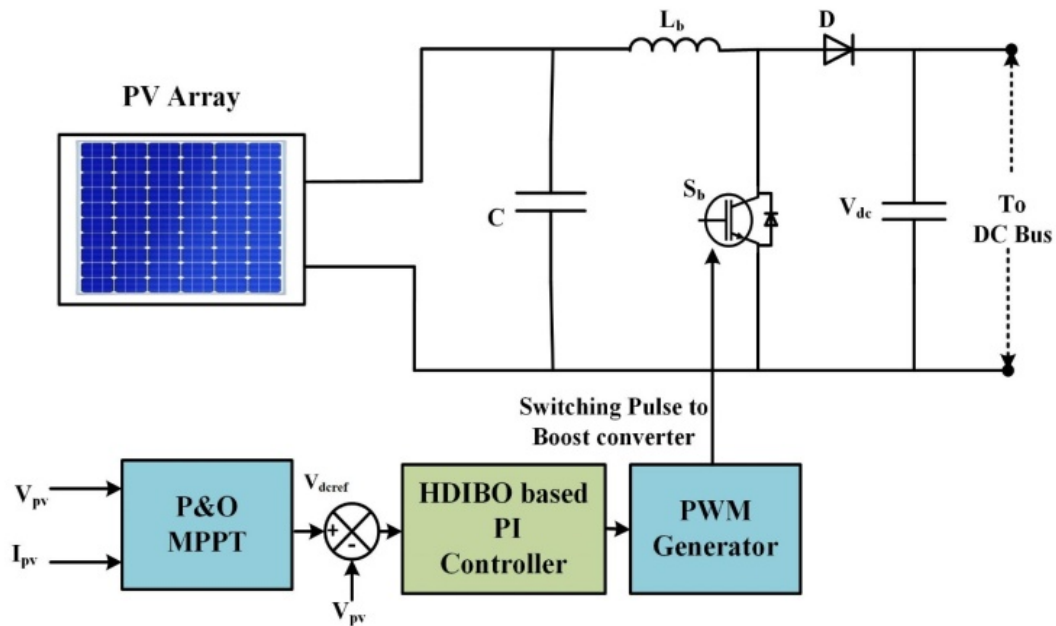


Figure 2:PV interface and its control

The boost converter employs an inductor to store energy, with its voltage drop changing in response to current variations. This configuration guarantees a controlled and elevated DC output for the load. A representation of the standard power circuit for a boost converter for PV power conversion is depicted in Figure 2. The boost converter employs solid-state components like power MOSFETs and diodes to act as switches. The capacitor and load are linked in a parallel arrangement, while the inductor is connected sequentially to the supply voltage source, ensuring a steady input current. Switch S is governed by PWM, achievable through time-based or frequency-based modulation. While time-based modulation is the typical choice due to its simplicity and constant frequency, frequency-based modulation offers a broader switch control frequency range, albeit demanding a more intricate low-pass LC filter design. The state space representation of the boost converter is presented in equation (3),

$$\begin{bmatrix} \dot{i}_L \\ \dot{v}_C \end{bmatrix} = \begin{bmatrix} 0 & -\frac{(1-d)}{L} \\ \frac{(1-d)}{C} & -\frac{1}{RC} \end{bmatrix} \begin{bmatrix} i_L \\ v_C \end{bmatrix} + \begin{bmatrix} \frac{1}{L} \\ 0 \end{bmatrix} V_s \quad (3)$$

Maximizing the energy output of photovoltaic (PV) modules remains a pivotal objective within solar power systems, prominently relying on the development of efficient Maximum Power Point Tracking (MPPT) algorithms. The Perturb and Observe (P&O) MPPT technique has gained widespread usage due to its straightforward yet effective approach. This method involves cyclically perturbing the functioning point of the PV scheme and subsequently observing the ensuing change in output power. This observed change guides the determination of the direction for the next perturbation iteration. However, the P&O method's efficiency can be hampered by oscillatory behavior around the maximum power point, leading to suboptimal energy extraction and potential strain on the PV system.

One technique for overcoming these constraints is to incorporate a PI controller with the P&O algorithm. The incorporation of PI control aims to refine the perturbation process by continually adjusting the perturbation magnitude based on the error among the real and desired operating points. By combining the strengths of both methods, namely P&O's simplicity and PI control's precise and consistent convergence, a more effective approach emerges. The PI controller introduces a feedback loop that continuously evaluates the system's performance, thus adapting the perturbation magnitude in a seamless manner. This adaptive feature significantly reduces the oscillations that typically plague the P&O algorithm, resulting in smoother and more constant monitoring of the highest power point.

The PI controller output for the MPPT (Duty cycle ( $D_{ref}$ )) of the PV systems is expressed in the following equation:

$$D_{ref} = K_{mp} \times (V_{ref} - V_{PV}) + K_{mi} \int (V_{ref} - V_{PV}) dt \quad (4)$$

## 2.2 Wind Energy Conversion System and its Control

The wind energy sector has witnessed remarkable advancements in recent years, notably in the design and operation of wind turbine systems. Figure 3 shows the details of the wind energy system and its control logic. A pivotal component of this progress is the permanent magnet

synchronous generator (PMSG) integrated into wind turbine setups. The PMSG's coupling with a rectifier marks a significant stride towards efficient energy conversion. The rectifier's role in transforming alternating current (AC) to direct current (DC) cannot be understated, as it forms the bridge between the generator and the energy storage system.

In this intricate setup, the DC bus assumes a pivotal role. For optimize the energy transformation process, a boost converter is employed to elevate the DC voltage to the desired DC bus voltage. This voltage amplification is integral for effective power transmission across the network.

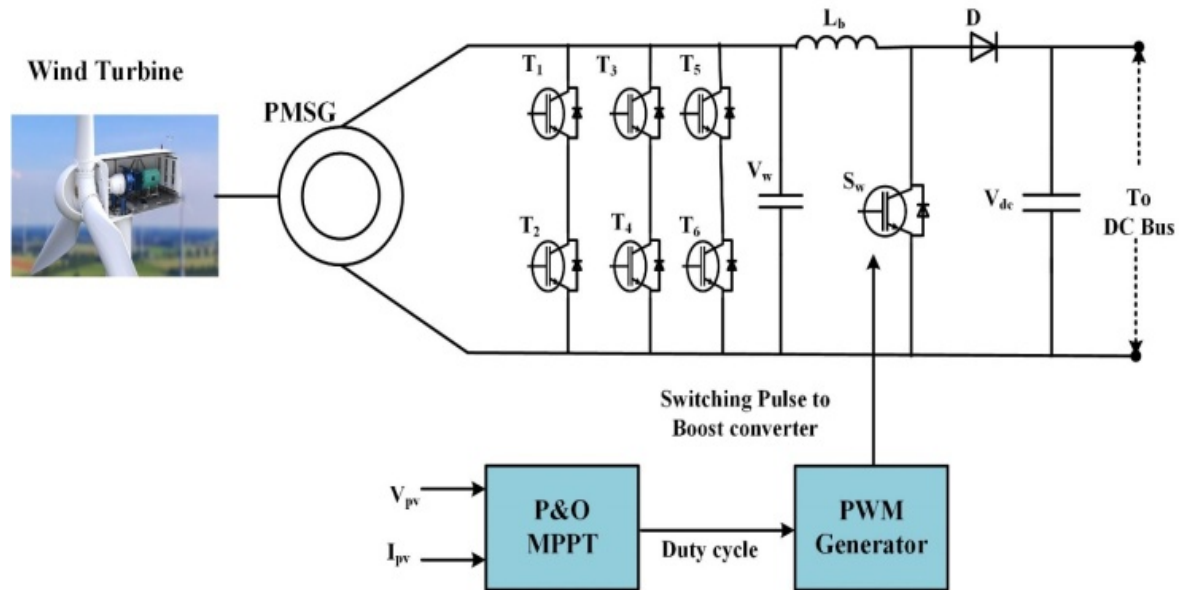


**Figure3:** Wind Energy and its interface System

The boost converter's significance lies not only in voltage augmentation but also in its seamless integration with the Maximum Power Point Tracking (MPPT) technique. The Perturb and Observe (P&O) MPPT algorithm is harnessed for its ability to extract maximum power from the wind turbine system. The algorithm actively gauges the system's operating point and adjusts the boost converter's parameters accordingly. By regulating the boost converter in tandem with the P&O MPPT algorithm, the wind turbine system can consistently operate at its peak efficiency, harnessing the optimal power output under varying wind conditions. This intricate interplay of components showcases the meticulous design and engineering that underpin modern wind turbine systems. The amalgamation of the PMSG, rectifier, boost converter, and MPPT algorithm epitomizes the fusion of innovative technologies geared towards enhancing energy conversion efficiency and ultimately contributing to the sustainable energy landscape.

### 2.3 Energy Storage Battery and its Control

In the realm of electric vehicle (EV) applications, a pivotal aspect lies in the integration of energy storage batteries to effectively manage power flow and enhance overall efficiency. Within this context, a bidirectional DC-DC converter plays a crucial role by establishing a connection between the energy storage battery and the common DC bus in the EV system. This dynamic

arrangement permits the battery to seamlessly charge or discharge energy as required by the vehicle's operation. Figure 4 shows the arrangement of the energy storage battery and its control.

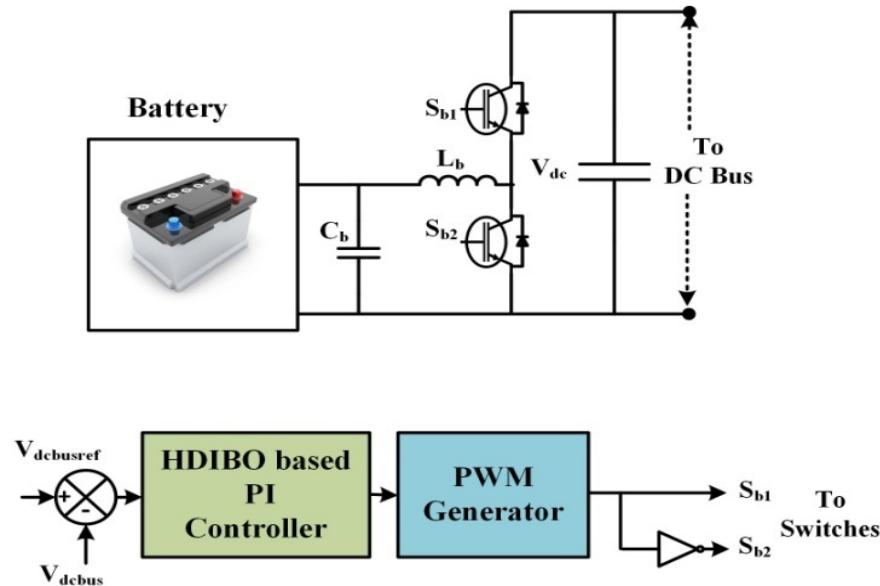


**Figure 4:**Energy storage battery and its control

Ensuring a stable and consistent voltage across the DC bus is paramount for the smooth functioning of the EV. To achieve this, a sophisticated DC bus voltage control method is employed, with a Proportional-Integral (PI) control technique at its core. This control strategy allows for precise monitoring of the DC bus voltage and facilitates real-time adjustments to the bidirectional DC-DC converter's operation. The PI controller within this setup serves as an intelligent supervisor, meticulously regulating the converter's behavior. It gauges the disparity between the actual DC bus voltage and the desired level and then responds proportionally through the proportional component. Additionally, the integral component ensures that any accumulated errors are effectively minimized over time, guaranteeing accurate and efficient voltage control. The seamless integration of these elements within the EV application holds paramount significance. As the electric vehicle navigates through varying power demands during its operation, the PI controller orchestrates timely and precise alterations to the bidirectional converter. The output equation for the PI controller is expressed in the following equation,

$$D_{ref} = K_{bp} \times (V_{dcbusref} - V_{dcbus}) + K_{bi} \int (V_{dcbusref} - V_{dcbus}) \quad (5)$$

This harmonized system ensures that energy flows optimally to and from the battery, contributing to extended battery life, improved vehicle range, and overall enhanced performance. The amalgamation of energy storage batteries, bidirectional DC-DC converters, and the PI control technique in the electric vehicle domain exemplifies the strides being made in sustainable transportation. This integration not only maximizes energy utilization but also reinforces the stability and dependability of EV systems, underscoring their pivotal role in the automotive industry's transition towards a greener future.

### 2.4 Electric Vehicle Battery and its Control

An electric vehicle's battery system is intricately designed to interface with a shared direct current (DC) bus through a bidirectional DC-DC converter, which plays a pivotal role in enabling efficient energy transfer between the battery and the bus. The bidirectional DC-DC converter serves as a crucial link that facilitates the rapid charging process of the electric vehicles (EV) battery while also enabling power flow from the battery to the bus, such as during vehicle to dc grid. Figure 5 shows the structure of the control of the electric vehicle battery.

The core of this system lies in the electric vehicle battery current control method, a sophisticated strategy aimed at ensuring optimal and swift charging of the EV battery. This control method hinges on the implementation of a Proportional-Integral (PI) control technique, a well-established control mechanism in engineering that aids in maintaining the desired battery current levels. The output equation for the PI controller is expressed in the following equation,

$$D_{ref} = K_{evp} \times (I_{evref} - I_{ev}) + K_{evi} \int (I_{evref} - I_{ev}) \quad (6)$$

By employing the PI control technique, the bidirectional DC-DC converter carefully regulates the current flowing into or out of the EV battery. During the charging phase, the converter adjusts its operations to guarantee that the battery receives the appropriate amount of current for quick and efficient charging. This not only minimizes charging time but also safeguards the battery from potential overcharging, enhancing its longevity.

The converter reverses its operation, allowing excess energy from the vehicle's momentum to be harvested and transferred back to the battery, thus increasing overall energy efficiency. This intricate system involving the bidirectional DC-DC converter and the PI-controlled battery current regulation mechanism underscores the pivotal role of advanced control techniques in optimizing the charging process of electric vehicle batteries.

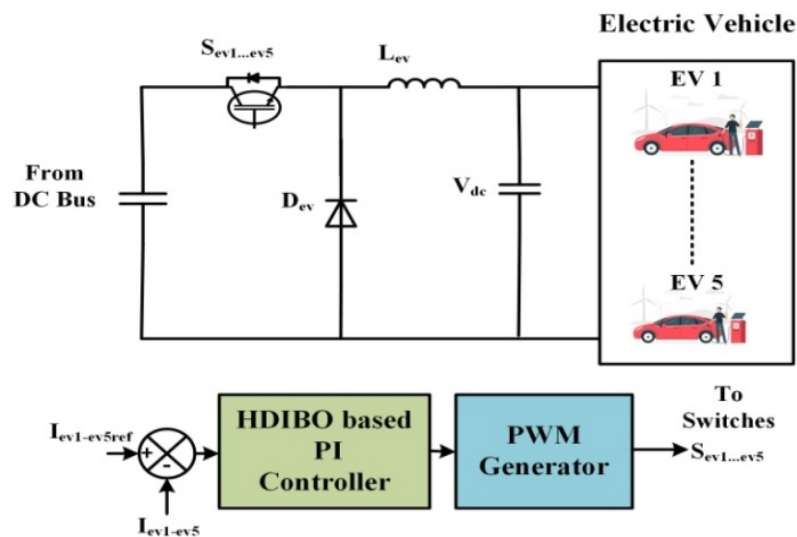


**Figure 5:**Electric vehicle battery and its control

This synergy of technology ultimately contributes to the expansion of electric vehicles' viability by enhancing their charging efficiency and overall performance.

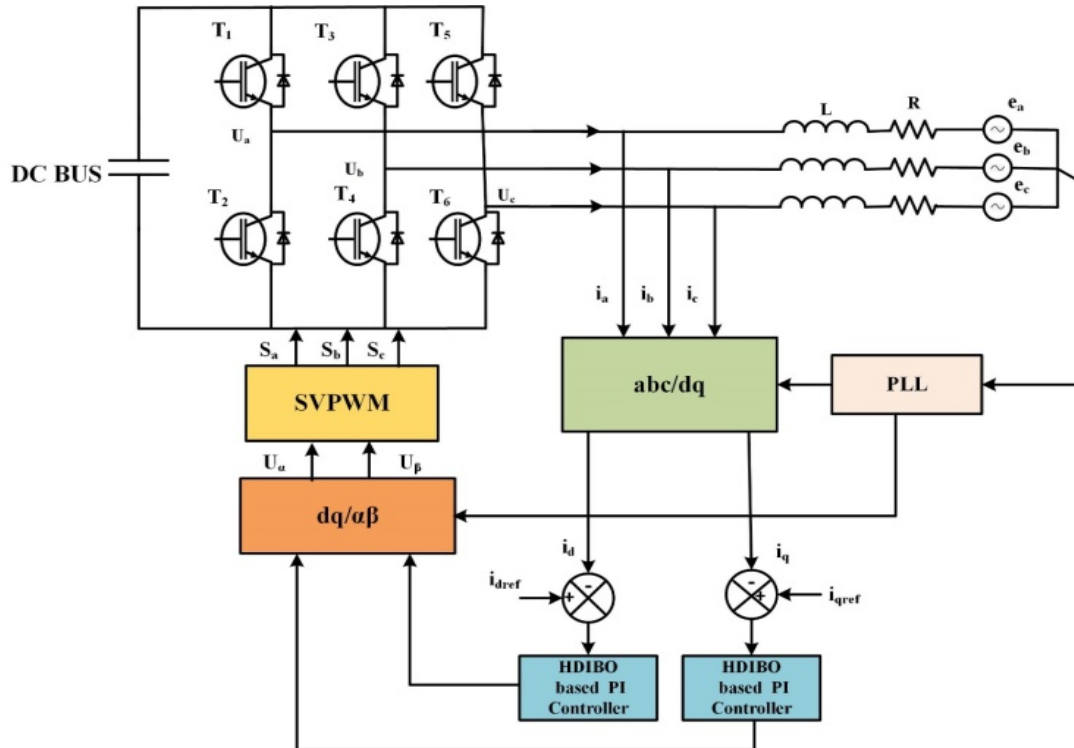


Figure 6:Control logic of the grid inverter

### 2.5 Computational Model of Grid Linked Inverter

Figure 6 shows the control logic of the grid inverter. When all possible shifting states of the voltage source converter are considered, there are eight options. The switching states of an inverter are defined as follows:

$$S_k = \begin{cases} 1(\text{Theupperarmison, thelowerarmisoff}) \\ 0(\text{Theupperarmison, thelowerarmison}) \end{cases} \quad (7)$$

The three-phase sequence is represented by  $k=a,b,c$ . The succeeding is a mathematical representation of a 3-phase static coordinate system inverter employing Kirchhoff's voltage law and switching function:

$$\begin{cases} Ri_a + L \frac{di_a}{dt} = u_{dc} \left( S_a - \frac{1}{3} \sum_{k=a,b,c} S_k \right) - e_a \\ Ri_b + L \frac{di_b}{dt} = u_{dc} \left( S_b - \frac{1}{3} \sum_{k=a,b,c} S_k \right) - e_b \\ Ri_c + L \frac{di_c}{dt} = u_{dc} \left( S_c - \frac{1}{3} \sum_{k=a,b,c} S_k \right) - e_c \end{cases} \quad (8)$$

Where  $i_a, i_b,$  and  $i_c$  are VSC current outputs,  $u_{dc}$  is the DC bus voltage, and  $e_a, e_b,$  and  $e_c$  are 3 phase voltages at the grid. The Clarke conversion is used to turn the three-phase static coordinate system into the system of coordinates, and the inverter voltages that result are as follows:

$$\begin{cases} u_\alpha = \sqrt{\frac{2}{3}} U_{dc} \left[ S_a - \frac{1}{2} (S_b + S_c) \right] \\ u_\beta = \frac{\sqrt{2}}{2} U_{dc} (S_b - S_c) \end{cases} \quad (9)$$

$$\begin{cases} u_\alpha = L \frac{di_\alpha}{dt} + Ri_\alpha + e_\alpha \\ u_\beta = L \frac{di_\beta}{dt} + Ri_\beta + e_\beta \end{cases} \quad (10)$$

Where  $u_\alpha$ ,  $u_\beta$  and  $i_\alpha$ ,  $i_\beta$  are the coordinate system VSC output voltages and currents, respectively. The grid voltages in the coordinate system are  $e_\alpha$ ,  $e_\beta$ . In the dq coordinate system, the inverter output powers are calculated by matching the grid voltage synthesizing vector E and the d-axis.

$$\begin{cases} P = \frac{3}{2} (e_d i_d + e_q i_q) = \frac{3}{2} E i_d \\ Q = \frac{3}{2} (e_q i_d - e_d i_q) = -\frac{3}{2} E i_q \end{cases} \quad (11)$$

P and Q have an exponential connection with active and reactive currents, respectively, according to (11). The resulting active and reactive power may be split and regulated individually by altering both the active and reactive currents independently.

## 2.6. Control of Grid Connected Inverter With PI Controller and Feed Forward Decoupling Control

A typical PWM inverter control approach known as feed forward decoupling control strategy based on double-loop PI regulation. The design of a DC voltage outer loop, a current inner loop, and PI regulators lies at its heart. Figure 6 depicts the construction of an inverter control method. Decoupling control is used to avoid mutual influence between the d and q axes in the current inner loop and to remove influence between active and reactive power.

$$\begin{cases} U_d = - \left( K_{ip} + \frac{K_{il}}{s} \right) (i_{dref} - I_d) + \omega L I_q + e_d \\ U_q = - \left( K_{ip} + \frac{K_{il}}{s} \right) (i_{qref} - I_q) + \omega L I_d + e_q \end{cases} \quad (12)$$

Where,  $K_{il}$  and  $K_{ip}$  are the proportional and integral regulation coefficients of the present inner loop PI regulators. SVPWM and feed forward decoupling control strategies are combined in the feed forward decoupling control of an inverter based on a PI regulator. The following is the control procedure: (1) Phase-locked loop is used to obtain the rotating flux position angle  $\theta$ ; (2)  $i_d$  and  $i_q$  are obtained by coordinate transformation; (3) according to the feedback currents  $i_{dref}$ ,  $i_{qref}$ , the PI controllers are used to control the current inner loop to obtain  $u_d$ ,  $u_q$ ; (4)  $u_d$  and  $u_q$  are transformed into  $u_\alpha$ ,  $u_\beta$  through the dq to  $\alpha\beta$  coordinate transformation; (5)  $u_\beta$  are input to the SVPWM module to generate PWM signals to control the inverter.

## 3. Human Driving Instruction-Based Optimization

This segment introduces the Human Driving Instruction-Based Optimization (HDIBO) random optimization approach, which replicates the human action of driving instruction to tune the parameters of the PI controller of the grid-connected renewable energy system-based electric

vehicle charging station. The HDIBO strategy was largely influenced by the instructor-training programmes and how individuals learn to drive at driving schools (Dehghani et al., 2022).

The three steps of HDIBO are statistically characterized as follows: practice, modeling of pupil conduct based on instructor tactics, and teaching from the driving instructor. Tuning of the PI controller problem is used to assess the efficacy of HDIBO in optimization. The optimization findings reveal that HDIBO was effective in providing adequate solutions to optimization issues through an appropriate mix of exploration and exploitation. This chapter introduces the Driving Training-Based Optimization random optimization algorithm. The simulation findings show that HDIBO beats three competing methods, such as particle swarm optimization, genetic algorithms, and grey wolf optimization, and is superior in optimization applications.

### 3.1 Driving Training-based Optimization:

The many phases of the suggested Driving Training Based Optimization (DTBO) technique are explained in this part, followed by an introduction to its mathematical modeling. Inspiration for HDIBO, its central concept. Driving teaching is a sophisticated way for educating new drivers and helping them improve their driving skills. An inexperienced driver has a choice of teachers when they sign up for driving school. The required training and instructions are then delivered to the inexperienced driver. The inexperienced driver makes an attempt to learn from and emulate the instructor's driving methods. Additionally, private driving lessons can aid novice drivers in improving their skills. Given these linkages and activities, there are a tonne of design options for optimizers. The mathematical representation of this process served as one of the primary sources of motivation for the development of HDIBO.

### 3.2 Mathematics Model of HDIBO

The members of the population metaheuristic known as HDIBO are driving instructors and pupils. The presented problem is defined by the population matrix in Eq. (13), and members of the HDIBO represent potential solutions. At the start of the implementation, the locations of these members are initialized at random using Eq. (14).

$$X = \begin{bmatrix} X_1 \\ \vdots \\ X_i \\ \vdots \\ X_N \end{bmatrix}_{N \times m} = \begin{bmatrix} X_{11} & \dots & X_{1j} & \dots & X_{1m} \\ \vdots & \ddots & \vdots & \ddots & \vdots \\ X_{i1} & \dots & X_{ij} & \dots & X_{im} \\ \vdots & \ddots & \vdots & \ddots & \vdots \\ X_{N1} & \dots & X_{Nj} & \dots & X_{Nm} \end{bmatrix}_{N \times m} \quad (13)$$

$$x_{i,j} = lb_j + r \cdot (ub_j - lb_j), i = 1, 2, \dots, N, j = 1, 2, \dots, m, \quad (14)$$

In figure 7, X represents the HDIBO population,  $X_i$  the  $i$ th candidate solution,  $X_{i,j}$  the value of the  $j$ th parameter identified by the  $i$ th candidate solution,  $N$  the size of the HDIBO population,  $m$  the number of problem variables,  $r$  an arbitrary number between  $[0, 1]$ , and  $lb_j$  and  $ub_j$  the upper and lower limits of the  $j$ th problem variable. Each proposed solution includes values for the issue variables, which are then used to evaluate the objective function. As a result, the value of the objective function corresponding to each alternative solution is determined. The aim function values are represented by the  $T_e$  vector in Eq. (15).

$$F = \begin{bmatrix} F_1 \\ \vdots \\ F_i \\ \vdots \\ F_N \end{bmatrix}_{N \times 1} = \begin{bmatrix} F(X_1) \\ \vdots \\ F(X_i) \\ \vdots \\ F(X_N) \end{bmatrix}_{N \times 1} \tag{15}$$

Where  $F_i$  is the required function value supplied by the  $i$ th alternative solution and  $F$  denotes the vector that represents the objective functions. The  $T_e$  values acquired for the goal function are the fundamental metric for judging the quality of prospective solutions. Based on a study of the objective function's findings, the group of members with the greatest value has been referred to as the most efficient member ( $X_{best}$ ). Because candidate replies are improved and updated at the end of each cycle, the best member must be replaced.

The key distinction between metaheuristic algorithms is how candidate solutions are updated. During the three unique phases of (i) driver-learner instruction by a driving trainer, (ii) learner-driver modeling utilizing operator skills, and (iii) learner-driver practice, potential answers are updated in HDIBO.

**Phase 1:** The driving teacher provides exploratory instruction. The driver learner chooses the driving teacher they want to work with, and that instructor then instructs them on driving throughout the first part of the HDIBO update. The top individuals of the HDIBO society are split between a small number of driving instructors and trainee drivers. After the choice of a driving teacher and mastery of their abilities, members of the general public will visit many websites around the search space. The HDIBO exploration assistance in the thorough search and identification of the optimum region will be strengthened as a result. As a consequence, this phase of the HDIBO upgrade validates the exploratory possibilities of this algorithm. Based on an evaluation of the target function's values, as stated in Eq. (16), the  $N$  participants in the HDIBO who will serve as driving instructors are determined in each iteration.

$$DI = \begin{bmatrix} DI_1 \\ \vdots \\ DI_i \\ \vdots \\ DI_{N_{DI}} \end{bmatrix}_{N_{DI} \times m} = \begin{bmatrix} DI_{11} & \dots & DI_{1j} & \dots & DI_{1m} \\ \vdots & \ddots & \vdots & \ddots & \vdots \\ DI_{i1} & \dots & DI_{ij} & \dots & DI_{im} \\ \vdots & \ddots & \vdots & \ddots & \vdots \\ DI_{N_{DI}1} & \dots & DI_{N_{DI}j} & \dots & DI_{N_{DI}m} \end{bmatrix}_{N_{DI} \times m} \tag{16}$$

The number of driving instructors, the instructor who drives the matrix, the  $i$ th driving trainer, the  $j$ th dimension, and the  $i$ th driving instructor (i.e.,  $DI_i$ ) are all indicated by the expression  $N_{DI} = 0.1 \cdot N \cdot (1 t/T)$ , where  $T$  is the total number of iterations. The computational modeling of this phase initially determines the new position for every participant in this HDIBO phase using Eq. (17). According to Eq. (18), position 10 takes the place of position 1 if doing so raises the objective function's value.

$$x_{i,j}^{P1} = \begin{cases} x_{i,j} + r \cdot (DI_{k_{ij}} - I \cdot x_{i,j}), & F_{DI_{k_i}} < F_i ; \\ x_{i,j} + r \cdot (x_{i,j} - DI_{k_{ij}}), & \text{otherwise,} \end{cases} \tag{17}$$

$$X_i = \begin{cases} X_i^{P1}, & F_i^{P1} < F_i; \\ X_i, & \text{otherwise,} \end{cases} \quad (18)$$

I represent a driving instructor who will train the  $i$ th member and is randomly selected.  $r$  signifies an arbitrary number in the range  $[0, 1]$ ,  $DI_{ki}$  symbolizes its  $j$ th dimension,  $DI_{ki,j}$  represents its value, and  $FDI_{ki}$  represents the objective function. According to HDIBO first phase,  $X_i^{P1}$  is the new determined rating for the  $i$ th applicant solution..

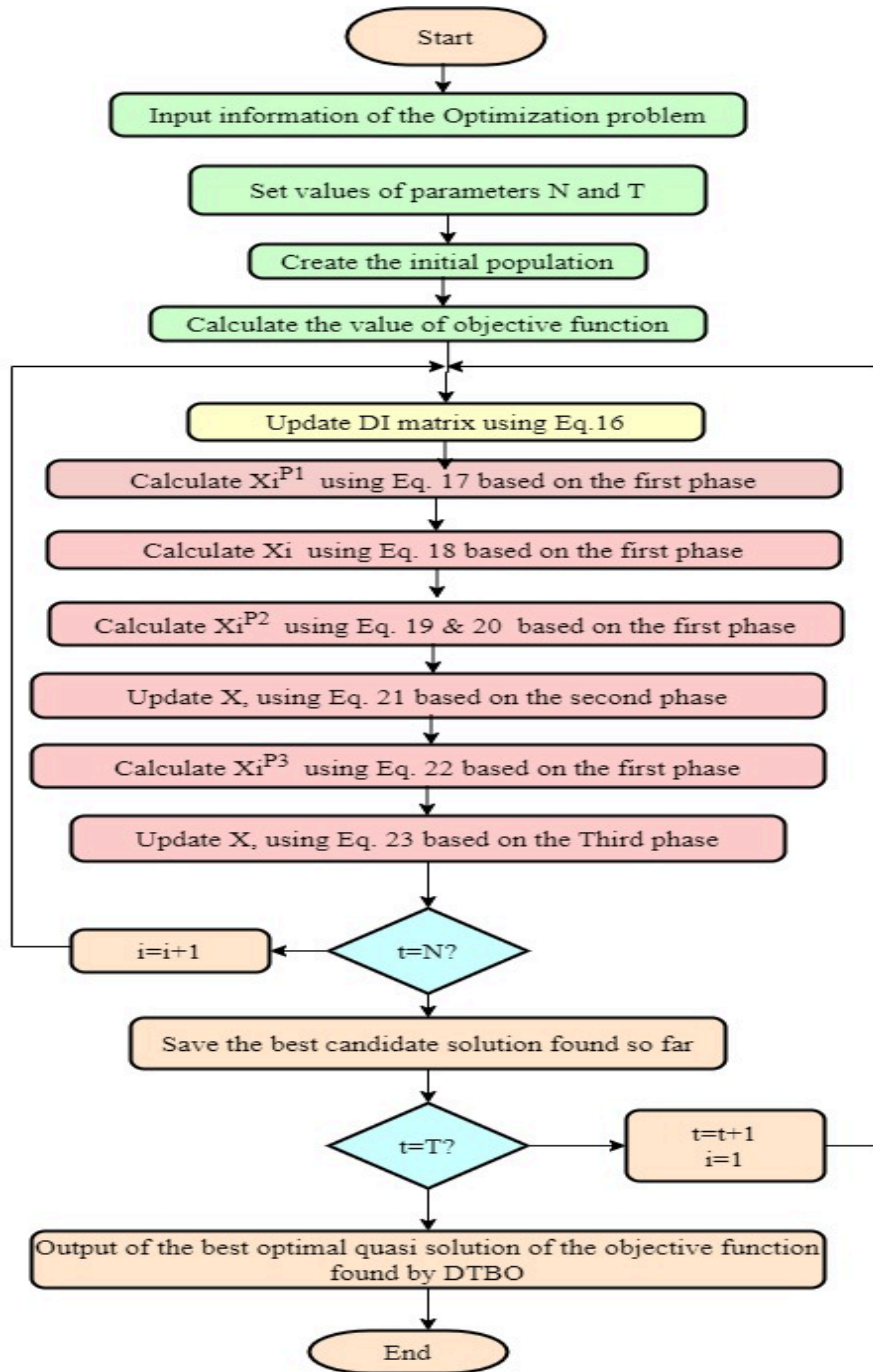


Figure 7: Flowchart of HDIBO -Based Metaheuristic Algorithm

**Phase 2: Exploration of the Student Driver's Teacher Abilities Modeling.** In the subsequent phase of the HDIBO update, the student driver attempts to imitate the instructor by copying all of the trainer's gestures and driving tactics. Through this process, the search space is traversed by different HDIBO members, accumulating the HDIBO exploration potential. In order to quantitatively replicate this notion, a new location is made based on a linear mixture of every participant with the teacher according to Eq. (19). If the new site raises the objective function's value, it will replace the old one, according to Eq. (20).

$$x_{i,j}^{P2} = P \cdot x_{i,j} + (1 - P) \cdot DI_{K_{i,j}} \quad (19)$$

$$X_i = \begin{cases} X_i^{P2}, & F_i^{P2} < F_i; \\ X_i, & \text{otherwise,} \end{cases} \quad (20)$$

$X_i^{P2}$  is the newly established rank for the  $i_{th}$  aspirant answer based on the subsequent phase of HDIBO,  $x_{i,j}^{P2}$  is its  $j_{th}$  dimensions, and  $P$  is the structure index assumed by

$$P = 0.01 + 0.9 \left(1 - \frac{t}{T}\right) \quad (21)$$

**Phase 3: Individual Practice (Exploitation).** The third stage of the HDIBO emphasizes each trainee driver's individual practice to strengthen and enhance their driving abilities. Each new driver strives to become a little bit closer to their greatest talents at this level. Each member can discover a more favorable position during this phase by doing a local hunt close to where they are presently placed. This level demonstrates how well HDIBO can leverage local search. In line with Eq. (22), a random site is initially established nearby each population member in the HDIBO phase's mathematical representation. Tenth, according to Eq. (23), the preceding position is replaced if this site raises the value of the objective function.

$$x_{i,j}^{P3} = x_{i,j} + (1 - 2r) \cdot R \cdot \left(1 - \frac{t}{T}\right) \cdot x_{i,j}, \quad (22)$$

$$X_i = \begin{cases} X_i^{P3}, & F_i^{P3} < F_i; \\ X_i, & \text{otherwise,} \end{cases} \quad (23)$$

The computational complexity of the HDBIO's issue presented here by constructing and setting up the HDIBO is  $O(N m)$ , where  $N$  is the total number of members and  $m$  is the total number of selection variables. Every cycle, the HDIBO members receive information in three stages. As a result, the compute cost of the HDIBO update methods is  $O(3NmT)$ , where  $T$  is the maximum number of iterations permitted by the methodology. The entire computational complexity of HDIBO is therefore  $O(N m(1 + 3T))$ .

### 3.2 Tuning of the PI Controller of the Grid Linked PV with Human Driving Instruction-Based Optimization

The parameter of the PI controller presented in the equation (4), (5), (6) and (12) such as  $K_{mp}, K_{bp}, K_{evp}, K_{ip}, K_{mi}, K_{bi}, K_{evi}$  and  $K_{ii}$  of the PI controller is optimized using Driving Instruction-Based Optimization with minimization of the following objective function,

For single stage grid connected PV system,

$$f(K_{mp}K_{bp}, K_{evp}, K_{ip}, K_{mi}, K_{bi}, K_{evi}K_{ii}) = \sqrt{\left(\frac{V_{ref}-V_{PV}}{N}\right)^2} + \sqrt{\left(\frac{V_{dcbusref}-V_{dcbus}}{N}\right)^2} + \sqrt{\left(\frac{I_{evref}-I_{ev}}{N}\right)^2} + \sqrt{\left(\frac{I_{dref}-I_d}{N}\right)^2} + \sqrt{\left(\frac{I_{qref}-I_q}{N}\right)^2} \quad (24)$$

Where N is the total amount of samples used in the optimization process. In the next section, optimization and simulation results of the proposed method with existing methods are explained.

### 3 Results and Discussions

The simulation outcomes of HDIBO optimization for tuning the PI controller in a grid-connected renewable energy system-based electric vehicle charging station are described in this section.

Table 2 presents a comprehensive overview of the specifications for a grid-connected renewable energy system that serves as an electric vehicle (EV) charging station. The first segment, labelled "PV Array," details the key attributes of the photovoltaic (PV) panels. Each individual panel is designed with a voltage of 36.19 V, a current of 8.43 A, and a power output of 305.08 W. The array configuration involves 11 panels in series, combined into 30 parallel strings, resulting in a remarkable total power capacity of 100 kW. A boost converter is integrated into this PV system, incorporating an inductor of 10.5 mH, a capacitor of 524  $\mu$ F, and operating at a frequency of 10 kHz. The subsequent section focuses on the "Wind Energy System," featuring a rated power output of 50 kW. The efficiency of the generator is highlighted at an impressive 90%. Similar to the PV setup, the wind energy system employs a boost converter, encompassing an inductor of 1.3 mH, a capacitor of 41 $\mu$ F, and operating at a frequency of 10 kHz.

Moving on to energy storage, the "Energy Storage Battery" component is equipped with a capacity of 40 kWhr operating at a nominal voltage of 300 V. This storage system integrates a bidirectional converter with an inductor of 10.5 mH, a capacitor of 524  $\mu$ F, and operates at a switching frequency of 10 kHz. Likewise, the "Electric Vehicle Battery," with a capacity ranging from 5 kWhr to 40 kWhr and a nominal voltage of 300 V, employs a bidirectional converter with identical specifications. The essential "DC link voltage" is set at 470 volts, serving as a pivotal conduit for energy transfer within the system. Lastly, the grid interface parameters include a voltage of 400 V and a frequency of 50 Hz, ensuring seamless integration with the larger power grid. Collectively, this table succinctly summarizes the intricate technical details of a grid-connected renewable energy system tailored to facilitate EV charging while harnessing solar and wind sources.

**Table 2:** Specification GA, PSO, Grey Wolf and Human Driving Instruction-Based Optimization

Genetic Algorithm		
	Description	Value
1	No. of Population	100
2	Maximum No. of Iteration	100
3	Selection Process	Roulette wheel
4	Cross Over rate	0.4
5	Mutation rate	0.05
Particle Swarm Optimization		
1	No. of Population	100
2	Maximum No. of Iteration	100
3	Inertial weight	0.9
4	Cognitive Weight	1.5
5	Social Weight	1.5
Grey Wolf Optimization		
1	No. of Population	100
2	Maximum No. of Iteration	100
Human Driving Instruction-Based Optimization		
1	No. of Population	100
2	Maximum No. of Iteration	100

Table 2 provides a concise breakdown of the specifications for four distinct optimization techniques: Particle Swarm Optimization (PSO) (Alhejji & Mosaad, 2021), Genetic Algorithm (GA) (Negi et al., 2022), Grey Wolf Optimization (Alremali et al., 2022), and Human Driving Instruction-Based Optimization. For the Genetic Algorithm, a population size of 100 individuals is established, and the algorithm undergoes a maximum of 100 iterations. The selection process is determined by a roulette wheel mechanism, with a crossover rate of 0.4 and a mutation rate of 0.05, influencing the exploration of solution space. In Particle Swarm optimization, the configuration comprises 100 particles in the population, with a maximum of 100 iterations. The optimization process considers an inertia weight of 0.9, along with cognitive and social weights both set at 1.5. These weights govern the balance between a particle's individual experience and the collective experience of the swarm. Grey Wolf Optimization follows a similar structure, with 100 wolves in the population and a maximum of 100 iterations. The algorithm imitates the social hierarchy of grey wolves and their hunting behaviour to optimize solutions. Lastly, Human Driving Instruction-Based Optimization involves a population size of 100 and a maximum of 100 iterations. This approach incorporates human expertise and driving behaviours to guide the optimization process. These four algorithms are used to tune the parameters of the PI controller in single and double-stage grid-connected PV systems with the minimization objective function

presented in equations (26) and (27). These algorithms are tested for 100 trials. The convergence graph of these four algorithms for PI controller tuning is shown in Figure 8.

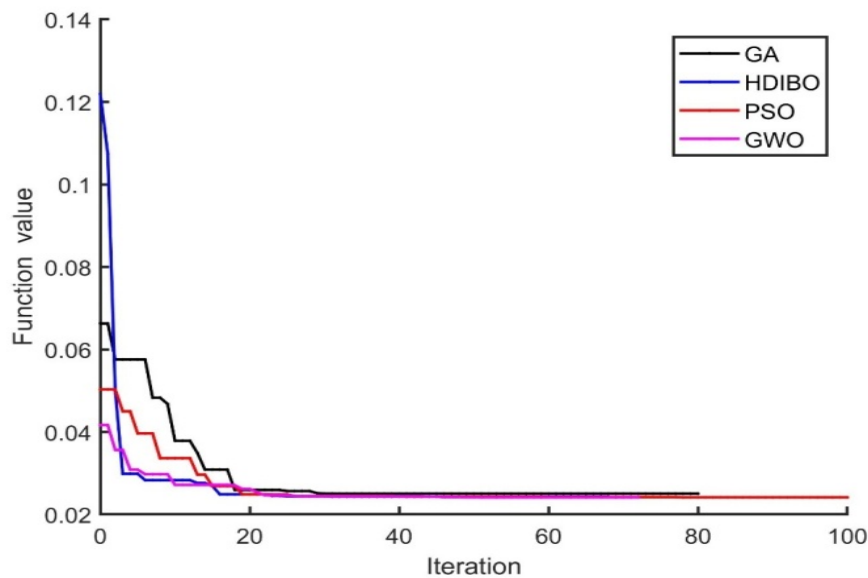


**Figure 8:** Convergence graph for PI controller optimization

**Table 3:** Tuned Parameter value of PI controller with GA, PSO, GWO and HDIBO for Grid connected Renewable energy system based Electric Vehicle charging station

Method	K <sub>mp</sub>	K <sub>mi</sub>	K <sub>bp</sub>	K <sub>bi</sub>	K <sub>evp</sub>	K <sub>e<sub>vi</sub></sub>	K <sub>ip</sub>	K <sub>ii</sub>	Mean	Standard Deviation	Best Fitness Value	Computation time (sec)
GA	0.042	0.458	0.0235	0.235	0.039	0.412	0.025	0.456	0.045	0.056	0.032	86.5
PSO	0.058	0.632	0.0854	0.145	0.0048	0.675	0.0056	0.656	0.056	0.034	0.031	74.3
GWO	0.0158	0.854	0.0412	0.524	0.0125	0.898	0.025	0.853	0.042	0.047	0.028	43.3
HDIBO	0.0854	0.254	0.0125	0.562	0.0814	0.222	0.086	0.2258	0.031	0.0023	0.025	28.2

Table 3 presents the tuned parameter values of PI controllers using various optimization methods, namely GA (Genetic Algorithm), PSO (Particle Swarm optimization), and GWO (Grey Wolf optimization). These controllers are applied to a grid-connected renewable energy system designed

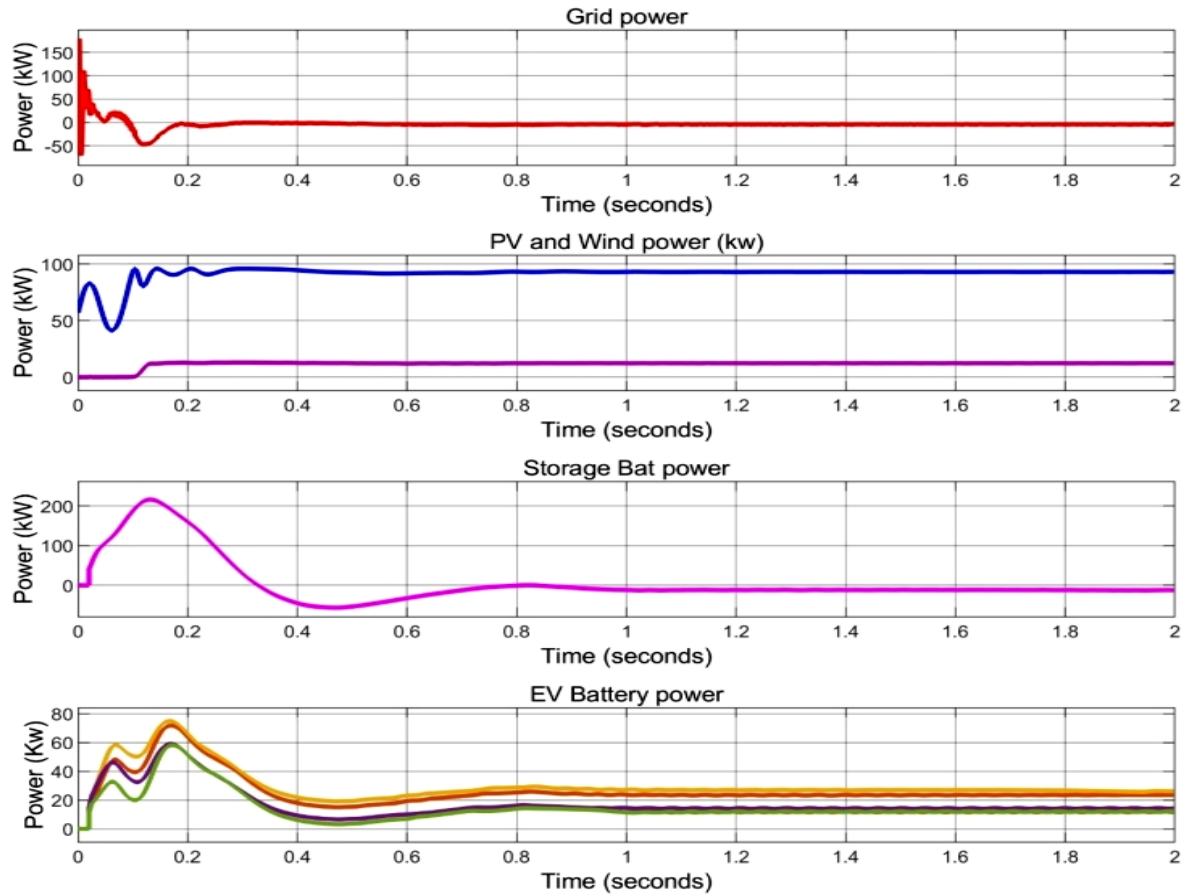
for an electric vehicle (EV) charging station. For the GA method, the controller parameters are set as follows: proportional gain (Kmp) of 0.042, integral gain (Kmi) of 0.458, derivative gain (Kdp) of 0.0235, and integral of derivative gain (Kdi) of 0.235. The mean values across iterations for these parameters are 0.045, 0.056, 0.032, and 86.5 seconds for computation time. In the case of the PSO method, the optimized parameters are found as follows: Kmp of 0.0058, Kmi of 0.632, Kdp of 0.0854, and Kdi of 0.145. The mean values are 0.056, 0.034, 0.031, and 74.3 seconds for computation time. The GWO method yields a Kmp of 0.0158, a Kmi of 0.854, a Kdp of 0.0412, and a Kdi of 0.524. The mean values for these parameters are 0.042, 0.047, 0.028, and 43.3 seconds for computation time. Finally, the HDIBO approach refines the parameters to achieve Kmp of 0.0854, Kmi of 0.254, Kdp of 0.0125, and Kdi of 0.562, with mean values of 0.031, 0.0023, 0.025, and 28.2 seconds for computation time. The table provides a comprehensive view of the optimized PI controller parameter values under each method, revealing the effectiveness of HDIBO in achieving improved parameter settings with lower mean and standard deviation values, contributing to efficient and stable control for the grid-connected renewable energy system used for EV charging.

**Table 4:** Operating conditions of a grid-connected renewable energy system-based electric vehicle charging station with varying irradiance, temperature, wind speed, and EV load details

SL.NO	Environmental Conditions			EV Load (kW)				
	Irradiance W/M2	Cell Temp (C)	Wind Speed (m/s)	EV1	EV2	EV3	EV4	EV5
1	0	25.541	5.23	27.4	0	0	0	0
2	0	25.377	5.01	11.8	13.7	0	0	0
3	0	25.253	4.82	0	0	0	0	0
4	0	25.199	4.81	34.4	19.5	0	0	0
5	0	25.222	4.88	12.7	18.2	14.0	0	0
6	0	25.721	5.68	13.8	11.8	29.4	30.4	0
7	130.841	27.681	7.07	15.9	14.3	14.0	29.4	31.5
8	395.214	30.023	7.55	14.8	16.9	30.4	15.6	29.4
9	636.433	32.41	7.74	15.6	15.1	11.7	30.4	25.5
10	828.791	34.494	7.82	15.0	18.2	13.8	30.4	25.5
11	954.926	35.908	7.79	12.7	20.8	15.1	28.4	25.5
12	1002.139	36.575	7.79	12.7	25.5	30.4	16.1	12.7
13	966.453	36.554	7.98	12.7	16.9	10.8	0	27.0
14	854.599	35.957	8.35	9.5	14.0	18.2	26.3	0
15	678.002	34.863	8.78	12.7	14.0	21.6	31.5	23.5
16	459.126	33.2	9.06	12.7	20.8	8.5	16.3	21.6
17	234.484	31.061	8.96	24.3	15.1	18.2	14.8	0
18	45.022	28.963	7.91	20.0	28.4	0	0	0

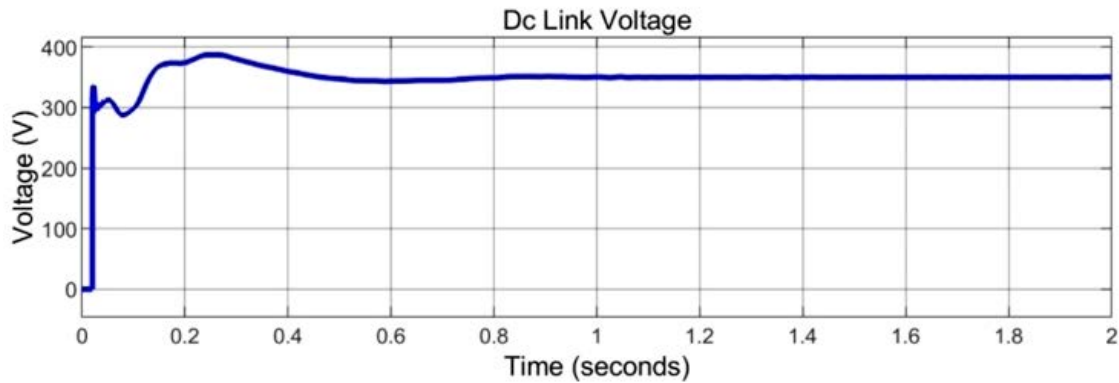
19	0	27.753	7.02	26.3	0	0	0	0
20	0	26.973	7.04	15.6	15.9	0	0	0
21	0	26.416	6.63	12.7	18.2	0	0	0
22	0	25.974	6.27	12.7	18.2	0	0	0
23	0	25.619	5.68	12.7	18.2	14.0	0	0
24	0	25.77	5.29	14.8	22.1	24.3	0	0

Table 4 presents an extensive overview of the operational conditions within a grid-connected renewable energy system that has been optimized to function as an electric vehicle (EV) charging station. The table incorporates a range of dynamic environmental factors such as irradiance, cell temperature, and wind speed and correlates them with the EV load details for different EV models (EV1 to EV5). For each distinct scenario, represented by the rows, the table documents the evolving environmental conditions—irradiance (measured in  $\text{W}/\text{m}^2$ ), cell temperature (in Celsius) and wind speed (in meters per second)—sourced from (NREL, 2023) and (NASA, 2023) respectively. Alongside these conditions, the table also records the corresponding EV load details (in kW) for each EV model at that specific moment. The comprehensive dataset showcased in the table captures the intricate interplay between external factors and EV charging demand. It reveals how the variability in environmental conditions, such as solar intensity, temperature, and wind speed, directly influences the EV load patterns across different EV models. This information is indispensable for effective energy management and load distribution within the grid-connected renewable energy system, enhancing the system's ability to respond adaptively to changing environmental dynamics and EV charging demands.



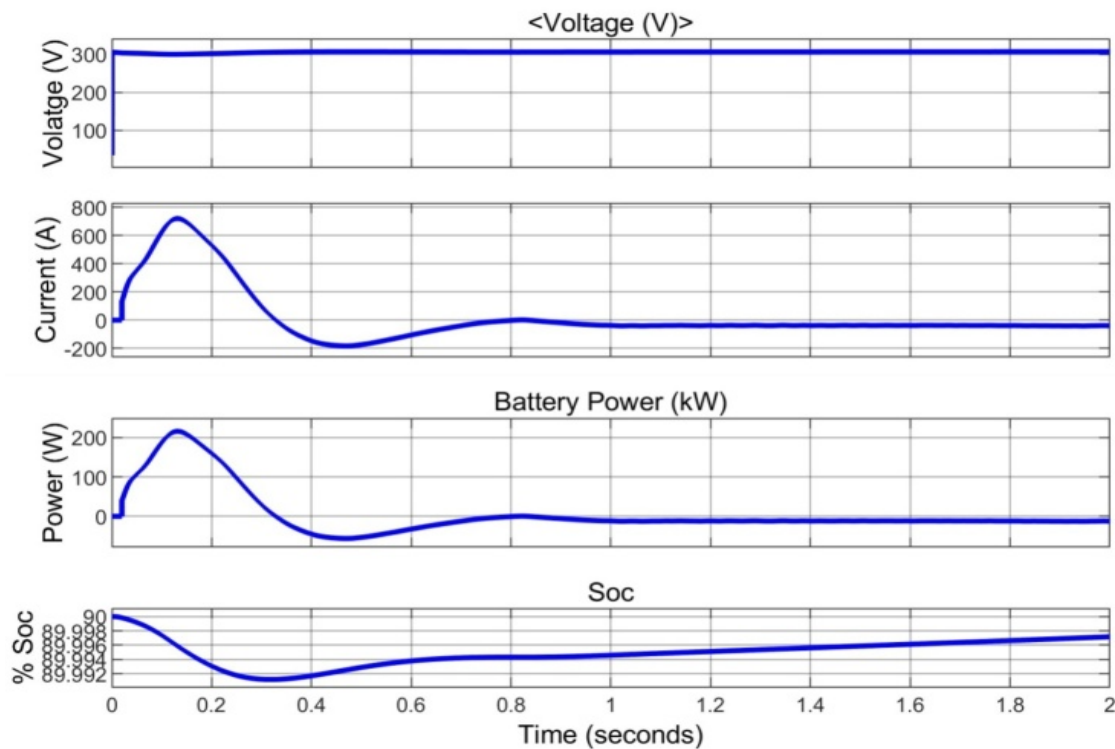
**Figure 9:**Power of the PV, Wind, and Storage Battery Power and EV battery at 24<sup>th</sup> hour data

Figure 9 presents data on the power generation and consumption of various energy sources and storage elements at the 24th hour. The result showcases the power outputs of photovoltaic (PV) panels, wind turbines, storage batteries, the grid, and electric vehicle (EV) batteries. The storage battery indicates a power output of -10.3 kW. The negative sign suggests that during this period, the battery is charging energy from the system. The grid exhibits a power output of -0.3 kW, potentially signifying a minor power deficit during this timeframe. This could indicate that the total demand is slightly surpassing the combined generation from all sources. Electric vehicles (EVs) play a dual role in this scenario. EV1, EV2, EV3, EV4, and EV5 are each shown with different power outputs: 12.7 kW, 25.5 kW, 30.4 kW, 16.1 kW, and 12.7 kW, respectively. These values likely represent the charging rates of the EV batteries at that specific hour. Positive values indicate that the EVs are drawing power from renewable energy sources. Overall, it captures a snapshot of the power dynamics in an integrated energy system at the 12th hour. It illustrates the contributions of renewable sources like PV and wind, the role of storage batteries in balancing supply and demand, and the interaction between the grid and electric vehicle charging.



**Figure 10:**DC Bus Voltages

Figure 10 provides information about the DC bus voltage within the energy system. The DC bus voltage is a key parameter that reflects the electrical potential difference at a specific point in the direct current (DC) circuit. Variations in the DC bus voltage can impact the overall stability and performance of the system. This figure likely presents a graphical representation of how the DC bus voltage changes over time, which is crucial for monitoring and managing the energy, flow within the system. The DC bus voltage is maintained at 350 V.



**Figure 11:** Storage Battery Voltage, Current, Power & SOC

Figure 11 presents multiple aspects of the storage battery's behaviour. It likely includes sub-figures or multiple lines depicting the variations in voltage, current, power output, and state of charge (SOC) of the storage battery over a certain period. Voltage illustrates the electrical potential

difference at the battery terminals and it maintained at 300 C; current depicts the flow of electric charge at -34 A; power represents the rate of energy transfer and is maintained at -10.3 KW; and SOC indicates the battery's energy capacity as a percentage of its maximum. This comprehensive view helps in assessing the battery's operational status, efficiency, and overall health.

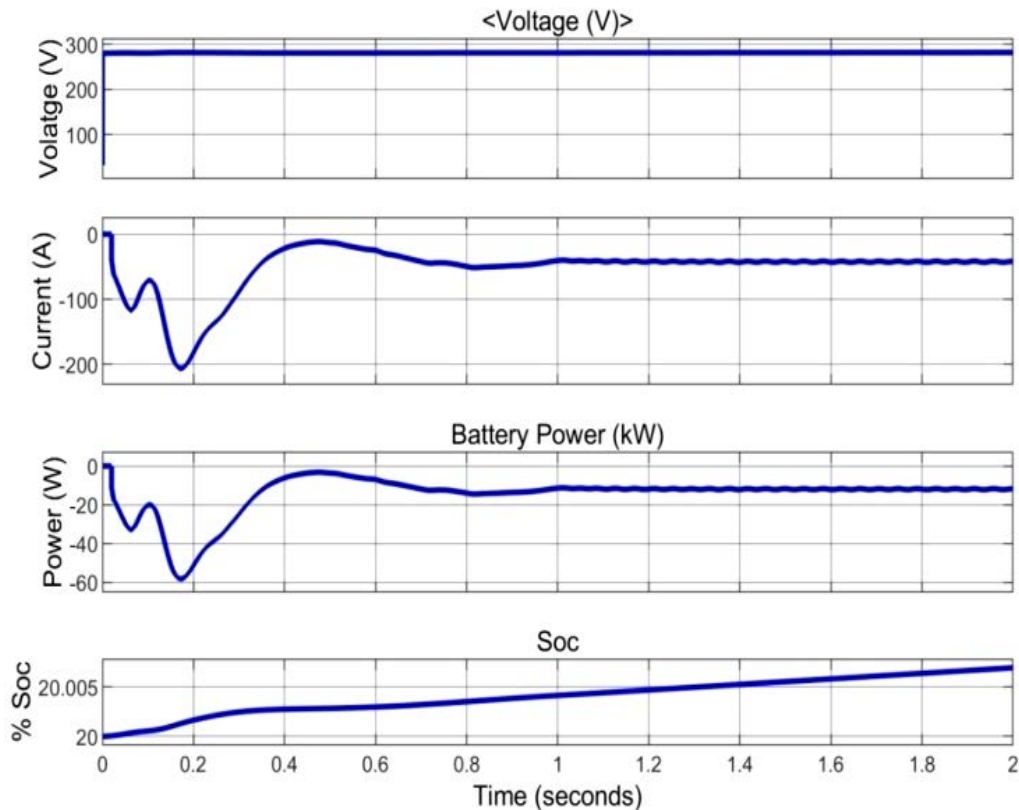


**Figure 12:** EV1 Battery Voltage, Current, Power & SOC

Figures 12 to 16 show the details of EV battery voltage, current, power, and SOC (EV1, EV2, EV3, EV4, and EV5). Each of these figures likely follows a similar pattern as Figure 12, but for different electric vehicles (EVs). They provide detailed insights into the behaviour of individual EV batteries. The figures might show how the voltage, current, power, and SOC values change for each EV battery over time. Monitoring these parameters is vital for understanding EV performance, charging patterns, and the overall condition of the batteries in the fleet.

All EVs will charge fully in 45 to 120 minutes. Collectively, these figures play a crucial role in providing a visual representation of various critical parameters within the energy system. They aid in assessing system stability, battery health, and the efficiency of energy transfer processes, thus enabling informed decision-making and effective management of the integrated energy and transportation system.

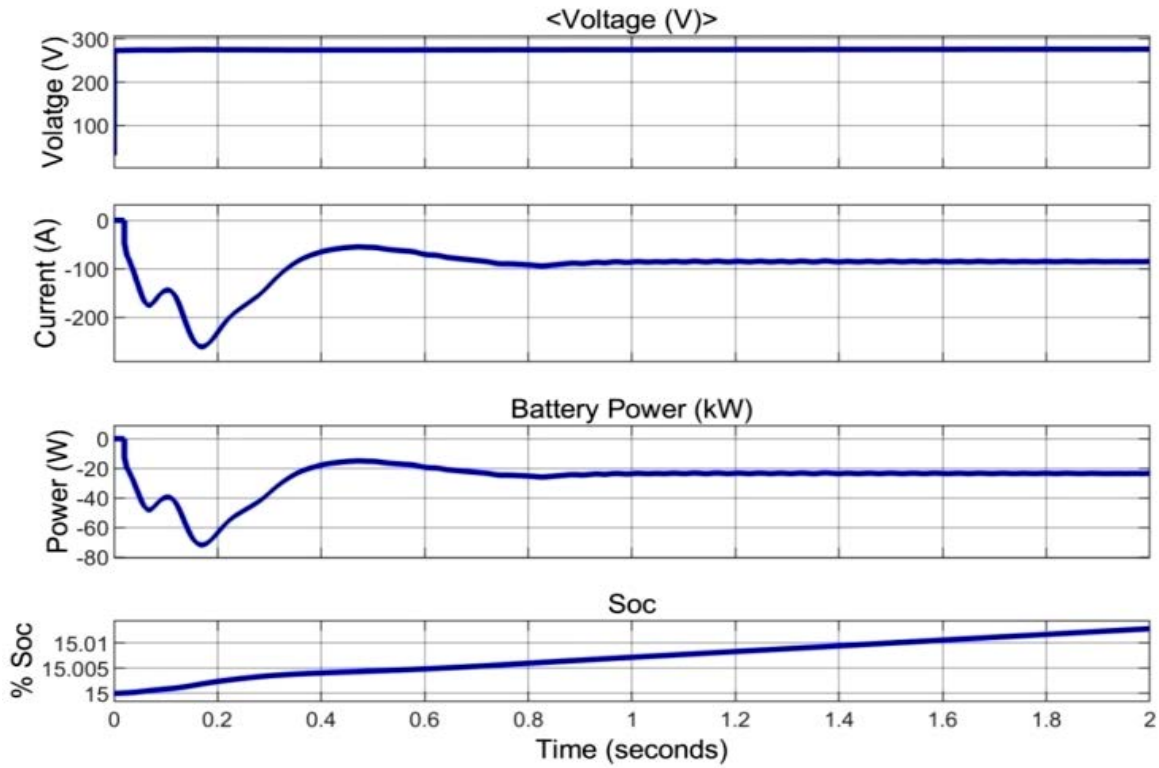


**Figure13:** EV2 Battery Voltage, Current, Power & SOC

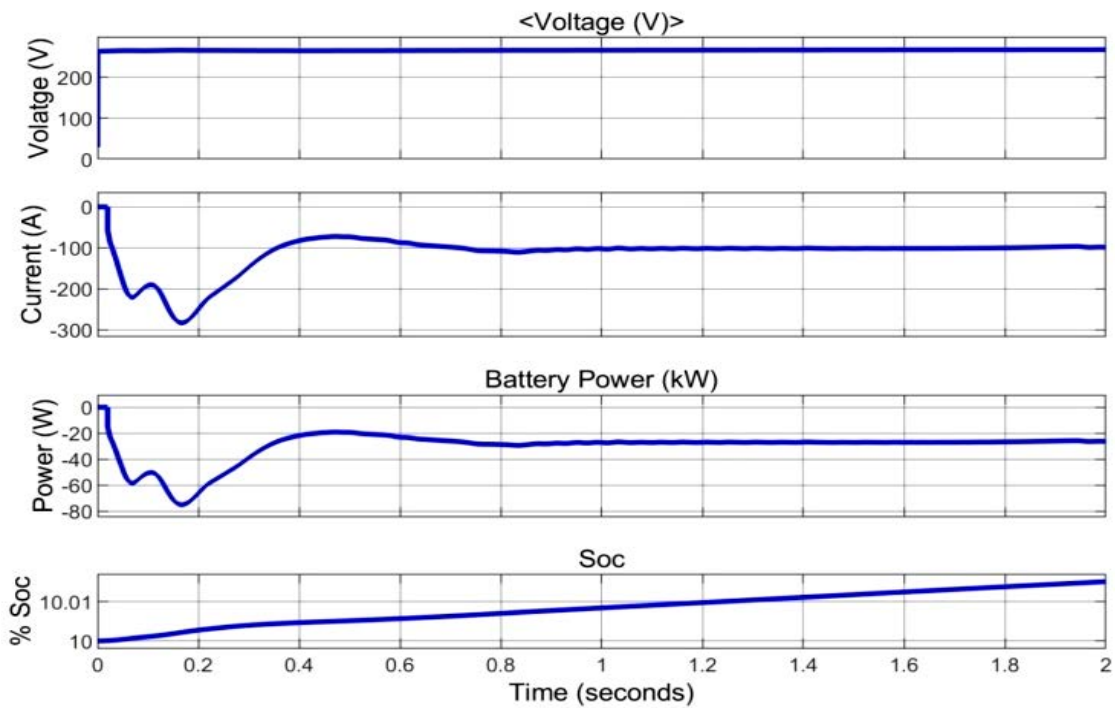


**Figure 14:** EV3 Battery Voltage, Current, Power & SOC

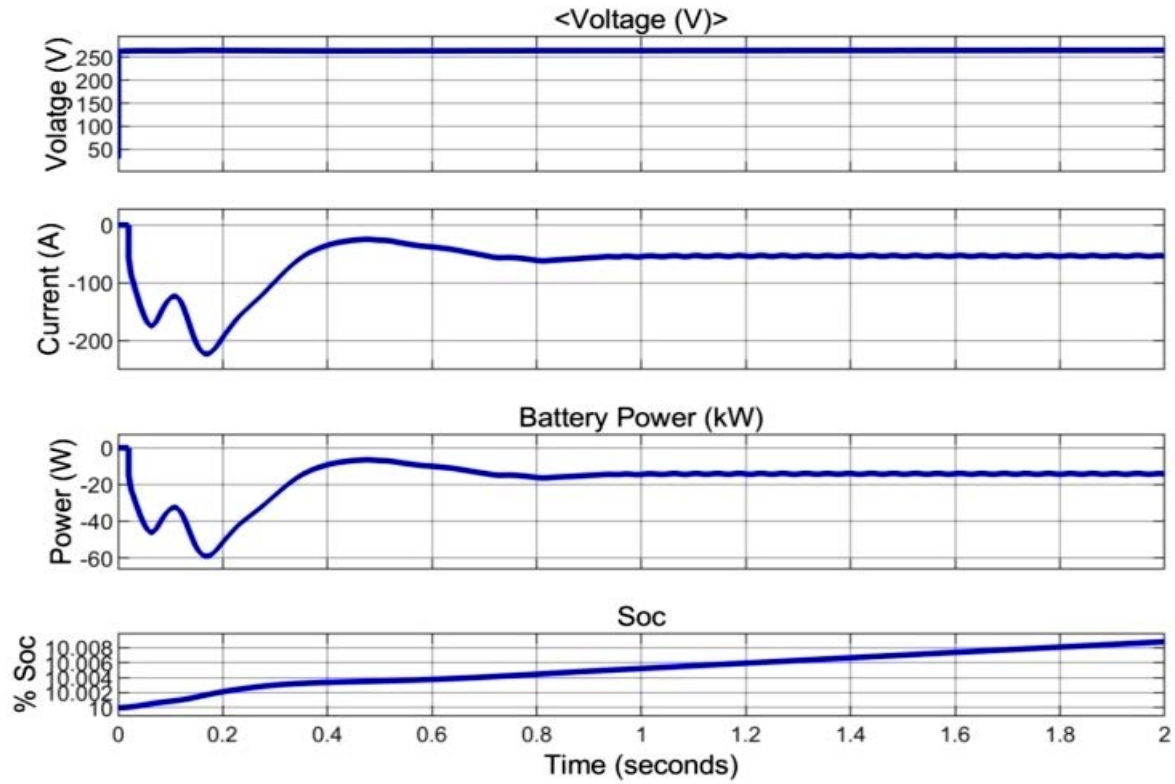


**Figure 15:** EV4 Battery Voltage, Current, Power & SOC

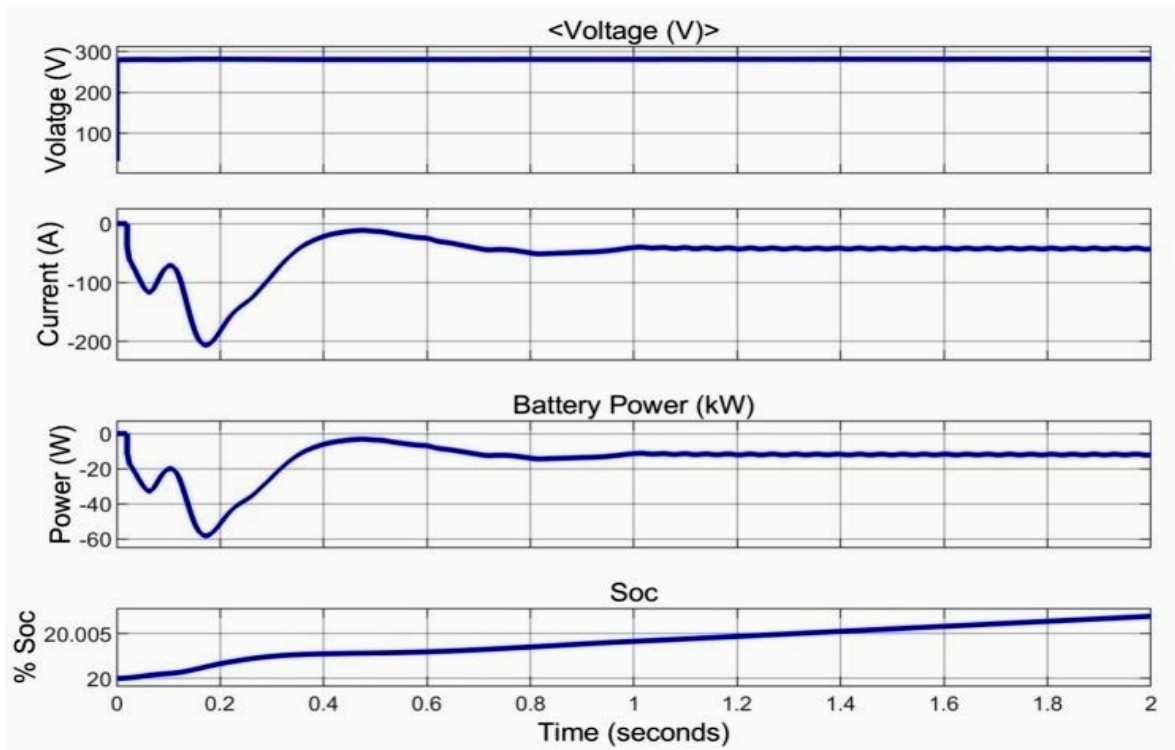


**Figure 16:** EV5 Battery Voltage, Current, Power & SOC

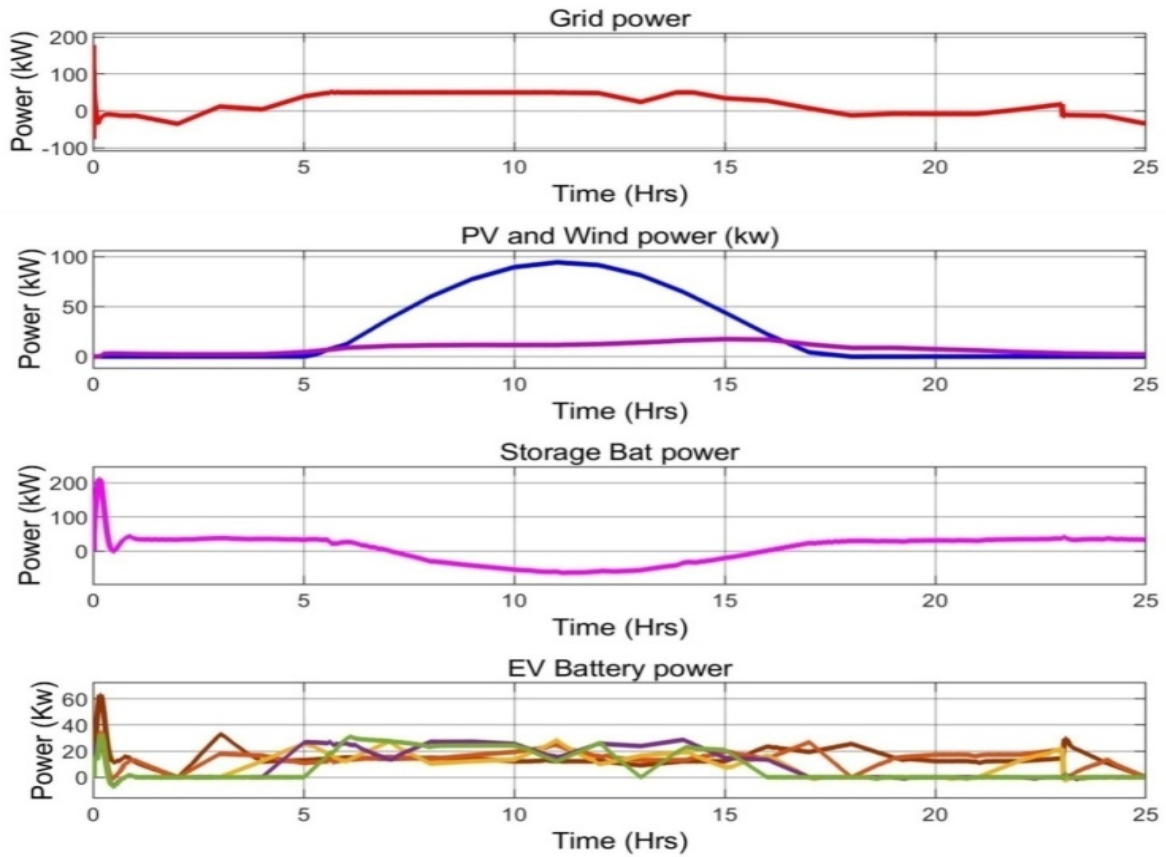


**Figure 17:** Power of the PV, Wind, Storage Battery and EV battery at 24 hours data

**Table 5:** Power of the PV, Wind, Storage Battery and EV battery at 24 hours data

SL. NO	POWERS (kW)			
	Grid power	PV Power	Wind Power	Battery Power
1	-13.0	0.0	2.7	38.2
2	-33.5	0.0	3.2	33.4
3	9.3	0.0	2.2	37.4
4	4.7	0.0	2.3	35.3
5	37.4	0.0	4.3	33.4
6	50.4	11.5	8.5	25.8
7	50.0	35.8	10.4	3.5
8	50.1	58.6	11.2	-28.2
9	49	76.8	11.6	-39.1
10	41.6	89	11.6	-39.3
11	8.4	94	11.5	-39.8
12	33.1	91.7	12.4	-39.8
13	39.6	81.8	13.9	-39.5

14	50.0	65.6	16.0	-37.4
15	35.7	45.0	17.3	-21.5
16	28.7	23.5	17.0	-0.2
17	8.1	5.1	12.4	22.9
18	-11.0	0.0	8.9	29.7
19	-7.6	-0.1	8.7	28.7
20	30.9	-0.1	7.4	30.9
21	-8.3	0.0	6.3	30.4
22	3.6	0.0	4.5	34.6
23	17.9	0.0	3.4	36.5
24	-12.5	0.0	2.6	34.5

Figure 18 and Table 5 synergistically provide an intricate portrayal of the power dynamics and energy interactions that unfold within a 24-hour span in an integrated energy system. These visual aids furnish invaluable insights into the intricate interplay among various power sources, storage mechanisms, and the charging requirements of electric vehicles (EVs). Figure 18, a visual representation, graphically elucidates the ebb and flow of power outputs across the 24-hour timeline. The x-axis denotes the duration, while the y-axis quantifies power in kilowatts (kW). Diverse lines on the graph delineate the contributions from discrete sources: grid power, photovoltaic (PV) power, wind power, and battery power. Moreover, the graph integrates the EV load demand, spotlighting the changing power requirements of EVs as the day progresses. Table 6, in addition to the graphical depiction, tabulates the power data for each source and EV load demand during distinct hours. Each row corresponds to a specific hour, with columns characterizing power sources (grid power, PV power, wind power, battery power) and EV load demands (EV1 to EV5). The table underscores the fluid nature of power generation, storage, and consumption over the 24-hour timeframe. Several enlightening takeaways stem from the furnished data: **Grid Power:** Negative grid power values (e.g., hours 1, 2, 18, and 19) signify instances of energy surplus, as excess energy is fed back into the grid during these periods. **PV and Wind Power:** The undulating patterns in PV and wind power mirror the availability of sunlight and wind, contributing to fluctuating energy inputs from these renewable sources. **Battery Power:** Fluctuations in battery power profile the charging and discharging cycles of the storage system. Energy accumulation transpires during surplus generation, while discharging addresses demand when generation wanes. **EV load demands:** The variable power requirements of EVs (EV1 to EV5) underscore shifting charging or discharging velocities as the day unfolds. Collectively, Figure 18 and Table 6 create a holistic snapshot of how renewable energy sources, grid power, and energy storage interface to cater to EV charging loads throughout time. This data proves pivotal for optimizing energy management, guaranteeing efficient exploitation of renewable resources, and maintaining equilibrium within the energy landscape. Furthermore, it underscores the dynamic nature of the system, shaped by multifarious influences on power generation, storage, and usage patterns. Notably, the integration of Human-Driven Instruction-Based optimization (HDIBO) serves as an approach that can enhance optimization outcomes. HDIBO leverages human insights

alongside algorithmic precision to dynamically respond to changing conditions, facilitating a more adaptable energy management strategy. This approach bridges the gap between theoretical algorithms and real-world complexities, resulting in optimized energy management, seamless grid integration, and efficient EV charging.

## 5. Conclusion

In conclusion, this research paper provides a comprehensive exploration of the power dynamics and energy interactions within an integrated energy system designed for electric vehicle (EV) charging stations. The study leverages advanced optimization techniques, including Genetic Algorithm (GA), Particle Swarm Optimization (PSO), Grey Wolf Optimization (GWO), and Human Driving Instruction-Based Optimization (HDIBO), to fine-tune the parameters of a Proportional-Integral (PI) controller in a grid-connected renewable energy system. The specifications of the system, outlined in Table 2, present a robust configuration that harnesses solar and wind energy sources to power EV charging. The simulation outcomes, as depicted in Figures 8 and 9, showcase the effectiveness of HDIBO in optimizing the PI controller parameters, resulting in enhanced control performance. The optimized parameters, detailed in Table 4, reflect the pivotal role of HDIBO in achieving superior parameter settings compared to other optimization methods, contributing to stable and efficient control of the energy system.

Furthermore, the research delves into the dynamic interplay between environmental conditions, EV load demands, and energy generation and consumption. The power profiles shown in Figures 10 to 16, along with the detailed data in Table 5, elucidate the impact of factors such as irradiance, temperature, wind speed, and EV charging loads on the system's performance. This insight is invaluable for understanding system behaviour, optimizing energy management, and ensuring efficient utilization of renewable resources. The crux of the research is encapsulated in Figure 18 and Table 6, which collectively provide a holistic overview of power generation, storage, and consumption over a 24-hour period. These visuals underscore the significance of renewable energy sources, grid power, and energy storage in meeting the demands of EV charging loads. Moreover, the integration of HDIBO, a human-guided optimization approach, enhances the adaptability of the system to changing conditions, highlighting the bridge between theoretical algorithms and real-world complexities.

In essence, this research paper not only presents a comprehensive framework for optimizing energy systems in EV charging stations but also emphasizes the importance of considering environmental factors and dynamic load demands. The results underscore the potential of advanced optimization techniques like HDIBO to enhance energy management strategies and pave the way for sustainable and efficient electric transportation powered by renewable resources.

**Authors' Contribution:** Sohankumar Prajapati. Conceptualization (lead); methodology, analysis, writing original draft. Sanjay Vyas: supervision, resources, project administration, writing review and editing,

**Funding Statement:** The author(s) received no financial support for the research, authorship, and/or publication of this article.

**Conflicts of Interest:** The authors declare no conflict of interest.

**Acknowledgments:** I wish to extend my utmost appreciation to my esteemed supervisors, Professor Sanjay Vyas, Prof. J.G. Jamnanai, and Dr. Bhavik Suthar, for their invaluable guidance and unwavering support throughout the entire research work. The individual's profound expertise and profound insights proved to be of immeasurable value in the formative stages of my research endeavour, facilitating the resolution of various obstacles encountered along the way.



Copyright by the author(s). This is an open-access article distributed under the Creative Commons Attribution License (CC BY-NC International,

<https://creativecommons.org/licenses/by/4.0/>), which allows others to share, make adaptations, tweak, and build upon your work non-commercially, provided the original work is properly cited. The authors can reuse their work commercially.

## References

Albert, J. R., Selvan, P., Sivakumar, P., & Rajalakshmi, R. (2022). An advanced electrical vehicle charging station using adaptive hybrid particle swarm optimization intended for renewable energy system for simultaneous distributions. *Journal of Intelligent and Fuzzy Systems*, 43(4), 4395–4407. <https://doi.org/10.3233/JIFS-220089>

Alhejji, A., & Mosaad, M. I. (2021). Performance enhancement of grid-connected PV systems using adaptive reference PI controller. *Ain Shams Engineering Journal*, 12(1), 541–554. <https://doi.org/10.1016/j.asej.2020.08.006>

Allouhi, A., & Rehman, S. (2023). Grid-connected hybrid renewable energy systems for supermarkets with electric vehicle charging platforms: Optimization and sensitivity analyses. *Energy Reports*, 9, 3305–3318. <https://doi.org/10.1016/j.egy.2023.02.005>

Alremali, F. A. M., Yaylacı, E. K., & Uluer, İ. (2022). Optimization of Proportional-Integral Controllers of Grid-Connected Wind Energy Conversion System Using Grey Wolf Optimizer based on Artificial Neural Network for Power Quality Improvement. *Advances in Science and Technology Research Journal*, 16(3), 295–305. <https://doi.org/10.12913/22998624/150401>

Amir, M., Zaheeruddin, Haque, A., Bakhsh, F. I., Kurukuru, V. S., & Sedighizadeh, M. (2023). Intelligent Energy Management scheme-based coordinated control for reducing peak load in grid-connected photovoltaic-powered electric vehicle charging stations. *IET Generation, Transmission & Distribution*. <https://doi.org/10.1049/gtd2.12772>

Biya, T. S., & Sindhu, M. R. (2019). Design and Power Management of Solar Powered Electric Vehicle Charging Station with Energy Storage System. *Proceedings of the 3rd International Conference on Electronics and Communication and Aerospace Technology, ICECA 2019*, 815–820. <https://doi.org/10.1109/ICECA.2019.8821896>

Cabrera-Tobar, A., Pavan, A. M., Blasuttigh, N., Petrone, G., & Spagnuolo, G. (2022). Real time

Energy Management System of a photovoltaic based e-vehicle charging station using Explicit Model Predictive Control accounting for uncertainties. *Sustainable Energy, Grids and Networks*, 31, 100769. <https://doi.org/10.1016/J.SEGAN.2022.100769>

Dai, Q., Liu, J., & Wei, Q. (2019). Optimal photovoltaic/battery energy storage/electric vehicle charging station design based on multi-agent particle swarm optimization algorithm. *Sustainability (Switzerland)*, 11(7). <https://doi.org/10.3390/su11071973>

de Oliveira-Assis, L., García-Triviño, P., Soares-Ramos, E. P. P., Sarrias-Mena, R., García-Vázquez, C. A., Ugalde-Loo, C. E., & Fernández-Ramírez, L. M. (2021). Optimal energy management system using biogeography based optimization for grid-connected MVDC microgrid with photovoltaic, hydrogen system, electric vehicles and Z-source converters. *Energy Conversion and Management*, 248(Mvdc). <https://doi.org/10.1016/j.enconman.2021.114808>

Dehghani, M., Trojovská, E., & Trojovský, P. (2022). A new human-based metaheuristic algorithm for solving optimization problems on the base of simulation of driving training process. *Scientific Reports*, 12(1), 1–21. <https://doi.org/10.1038/s41598-022-14225-7>

Filote, C., Felseghi, R. A., Raboaca, M. S., & Aşchilean, I. (2020). Environmental impact assessment of green energy systems for power supply of electric vehicle charging station. *International Journal of Energy Research*, 44(13), 10471–10494. <https://doi.org/10.1002/er.5678>

Garcia-Trivino, P., De Oliveira-Assis, L., Soares-Ramos, E. P. P., Sarrias-Mena, R., Garcia-Vazquez, C. A., & Fernandez-Ramirez, L. M. (2023). Supervisory Control System for a Grid-Connected MVDC Microgrid Based on Z-Source Converters With PV, Battery Storage, Green Hydrogen System and Charging Station of Electric Vehicles. *IEEE Transactions on Industry Applications*, 59(2), 2650–2660. <https://doi.org/10.1109/TIA.2023.3233556>

Glenn, J. A., & Alavandar, S. (2023). Hybrid Optimized PI Controller Design for Grid Tied PV Based Electric Vehicle. *Intelligent Automation and Soft Computing*, 36(2), 1523–1545. <https://doi.org/10.32604/iasc.2023.033545>

Hassoune, A., Khafallah, M., Mesbahi, A., & Bouragba, T. (2019). Optimization Techniques for DC Bus Voltage Balancing in a PV Grid System Based EVs Charging Station. *Advances in Science, Technology and Innovation*, 123–131. [https://doi.org/10.1007/978-3-030-05276-8\\_14](https://doi.org/10.1007/978-3-030-05276-8_14)

Hassoune, Abdelilah, Khafallah, M., Mesbahi, A., & Bouragba, T. (2020). Improved control strategies of electric vehicles charging station based on grid tied PV/battery system. *International Journal of Advanced Computer Science and Applications*, 11(3), 116–124. <https://doi.org/10.14569/ijacsa.2020.0110314>

Karmaker, A. K., Hossain, M. A., Pota, H. R., Onen, A., & Jung, J. (2023). Energy Management System for Hybrid Renewable Energy-Based Electric Vehicle Charging Station. *IEEE Access*, 11(February), 27793–27805. <https://doi.org/10.1109/ACCESS.2023.3259232>

Khan, W., Ahmad, F., & Alam, M. S. (2019). Fast EV charging station integration with grid ensuring optimal and quality power exchange. *Engineering Science and Technology, an International Journal*, 22(1), 143–152. <https://doi.org/10.1016/j.jestch.2018.08.005>

Leonori, S., Rizzoni, G., Frattale Mascioli, F. M., & Rizzi, A. (2021). Intelligent energy flow management of a nanogrid fast charging station equipped with second life batteries. *International*

*Journal of Electrical Power & Energy Systems*, 127, 106602.  
<https://doi.org/10.1016/J.IJEPES.2020.106602>

Li, C., Zhang, L., Ou, Z., Wang, Q., Zhou, D., & Ma, J. (2022). Robust model of electric vehicle charging station location considering renewable energy and storage equipment. *Energy*, 238. <https://doi.org/10.1016/j.energy.2021.121713>

Li, Y., Mohammed, S. Q., Nariman, G. S., Aljojo, N., Rezvani, A., & Dadfar, S. (2020). Energy management of microgrid considering renewable energy sources and electric vehicles using the backtracking search optimization algorithm. *Journal of Energy Resources Technology, Transactions of the ASME*, 142(5). <https://doi.org/10.1115/1.4046098>

Ma, C. T. (2019). System planning of grid-connected electric vehicle charging stations and key technologies: A review. *Energies*, 12(21). <https://doi.org/10.3390/en12214201>

Mateen, S., Amir, M., & Haque, A. (2023). *Ultra-Fast Charging of Electric Vehicles: An Integrated Review of Advancements in Power Electronics Converter Topologies, Route of Grid Stability and Optimal Battery Consideration*.

Mohamed, A. A. S., El-Sayed, A., Metwally, H., & Selem, S. I. (2020). Grid integration of a PV system supporting an EV charging station using Salp Swarm Optimization. *Solar Energy*, 205(January), 170–182. <https://doi.org/10.1016/j.solener.2020.05.013>

Narasipuram, R. P., & Mopidevi, S. (2021). A technological overview & design considerations for developing electric vehicle charging stations. *Journal of Energy Storage*, 43. <https://doi.org/10.1016/j.est.2021.103225>

NASA. (2023). *ArcGIS Web Application*. <https://power.larc.nasa.gov/data-access-viewer/>, NASA Gov. (accessed October 16, 2023).

Negi, P., Pal, Y., & Leena, G. (2022). Performance enhancement of grid-connected photovoltaic systems using Ant Lion optimisation and Genetic Algorithm-based optimisation techniques. *Cognitive Computation and Systems*, 4(3), 273–283. <https://doi.org/10.1049/ccs2.12058>

NREL. (2023). *SOLAR RESOURCE DATA*. NREL, NREL. <https://pvwatts.nrel.gov/>, (accessed October 16, 2023).

Penchalaiah, T., Hema Nagalatha, K., Aravind, M., Manikanta, K., Rakesh, K., & Vineela, N. (2023). Enhancing Harmonic Reduction of Grid Connected Wind-Solar PV Charging Station using Neural Network Controller. *International Conference on Sustainable Computing and Smart Systems, ICSCSS 2023 - Proceedings*, 1263–1270. <https://doi.org/10.1109/ICSCSS57650.2023.10169725>

Quddus, M. A., Kabli, M., & Marufuzzaman, M. (2019). Modeling electric vehicle charging station expansion with an integration of renewable energy and Vehicle-to-Grid sources. *Transportation Research Part E: Logistics and Transportation Review*, 128(May 2018), 251–279. <https://doi.org/10.1016/j.tre.2019.06.006>

Ray, P., Bhattacharjee, C., & Dhenuvakonda, K. R. (2022). Swarm intelligence-based energy management of electric vehicle charging station integrated with renewable energy sources. *International Journal of Energy Research*, 46(15), 21598–21618. <https://doi.org/10.1002/er.7601>

Saleh, B., Yousef, A. M., Ebeed, M., Abo-Elyousr, F. K., Elnozahy, A., Mohamed, M., & Abdelwahab, S. A. M. (2021). Design of PID Controller with Grid Connected Hybrid Renewable Energy System Using Optimization Algorithms. *Journal of Electrical Engineering and Technology*, 16(6), 3219–3233. <https://doi.org/10.1007/s42835-021-00804-7>

Sayed, K., Abo-Khalil, A. G., & Alghamdi, A. S. (2019). Optimum resilient operation and control DC microgrid based electric vehicles charging station powered by renewable energy sources. *Energies*, 12(22). <https://doi.org/10.3390/en12224240>

Sharma, P., & Chinnappa Naidu, R. (2023). Optimization techniques for grid-connected PV with retired EV batteries in centralized charging station with challenges and future possibilities: A review. *Ain Shams Engineering Journal*, 14(7), 101985. <https://doi.org/10.1016/j.asej.2022.101985>

Singh, S., Chauhan, P., & Singh, N. J. (2021). Feasibility of Grid-connected Solar-wind Hybrid System with Electric Vehicle Charging Station. *Journal of Modern Power Systems and Clean Energy*, 9(2), 295–306. <https://doi.org/10.35833/MPCE.2019.000081>

Thangam, T., & Kalifullah, A. H. H. (2023). Type 2 intelligent controller for grid-tied solar electric vehicle charging stations: Novel controller for PV FED grid-tied EV chargers. *Opportunities and Challenges in Climate-Friendly Clean Water and Energy Technologies*, 218–243. <https://doi.org/10.4018/978-1-6684-7303-0.ch010>

Wu, Y., Wang, Z., Huangfu, Y., Ravey, A., Chrenko, D., & Gao, F. (2022). Hierarchical Operation of Electric Vehicle Charging Station in Smart Grid Integration Applications — An Overview. *International Journal of Electrical Power and Energy Systems*, 139. <https://doi.org/10.1016/j.ijepes.2022.108005>

Yu, H., Niu, S., Shang, Y., Shao, Z., Jia, Y., & Jian, L. (2022). Electric vehicles integration and vehicle-to-grid operation in active distribution grids: A comprehensive review on power architectures, grid connection standards and typical applications. *Renewable and Sustainable Energy Reviews*, 168. <https://doi.org/10.1016/j.rser.2022.112812>

Zandrazavi, S. F., Guzman, C. P., Pozos, A. T., Quiros-Tortos, J., & Franco, J. F. (2022). Stochastic multi-objective optimal energy management of grid-connected unbalanced microgrids with renewable energy generation and plug-in electric vehicles. *Energy*, 241. <https://doi.org/10.1016/j.energy.2021.122884>

Zheng, P., Fang, Z., Li, H., Pan, Y., Luo, D., & Zhang, Z. (2022). Multi-objective optimization of hybrid energy management system for expressway chargers. *Journal of Energy Storage*, 54(July), 105233. <https://doi.org/10.1016/j.est.2022.105233>

## About the Author



Prof. Sohankumar Prajapati is currently pursuing a Ph.D. in the Electrical Engineering department of Kadi Sarva Vishwavidyalaya, Gandhinagar, Gujarat, India. He is working as an assistant professor in the department of electrical engineering at Government Engineering College, Patan. He studied at L.D. College of Engineering, Ahmedabad, and received his master's from L.D.R.P. Institute of Technology and Research, Gandhinagar, Gujarat, India. He had 18 years of teaching experience prior to pursuing a Ph.D. He is a lifetime member of ISTE. The professor is the author of two books, among them: S.G. Prajapati and Sanjay Vyas, Basic Electrical Engineering, Synergy Publication, first edition 2018. He delivered more than 24 expert lectures in the fields of renewable energy and electrical vehicles on national and international platforms. He has a patent on the title "An Internet of Things-Based Battery Life Estimation System for Electric Vehicles", Application No. 202221067140 A, and a publication date of December 2, 2022.